Journal of Computational Neuroscience (2019) 46:233–256
https://doi.org/10.1007/s10827-019-00713-9

A computational model of large conductance voltage and calcium activated potassium channels: implications for calcium dynamics and electrophysiology in detrusor smooth muscle cells

Suranjana Gupta[1] · **Rohit Manchanda**[1]

Received: 11 September 2018 / Revised: 14 February 2019 / Accepted: 19 February 2019 / Published online: 25 April 2019

Abstract

The large conductance voltage and calcium activated potassium (BK) channels play a crucial role in regulating the excitability of detrusor smooth muscle, which lines the wall of the urinary bladder. These channels have been widely characterized in terms of their molecular structure, pharmacology and electrophysiology. They control the repolarising and hyperpolarising phases of the action potential, thereby regulating the firing frequency and contraction profiles of the smooth muscle. Several groups have reported varied profiles of BK currents and I-V curves under similar experimental conditions. However, no single computational model has been able to reconcile these apparent discrepancies. In view of the channels' physiological importance, it is imperative to understand their mechanistic underpinnings so that a realistic model can be created. This paper presents a computational model of the BK channel, based on the Hodgkin-Huxley formalism, constructed by utilising three activation processes — membrane potential, calcium inflow from voltage-gated calcium channels on the membrane and calcium released from the ryanodine receptors present on the sarcoplasmic reticulum. In our model, we attribute the discrepant profiles to the underlying cytosolic calcium received by the channel during its activation. The model enables us to make heuristic predictions regarding the nature of the sub-membrane calcium dynamics underlying the BK channel's activation. We have employed the model to reproduce various physiological characteristics of the channel and found the simulated responses to be in accordance with the experimental findings. Additionally, we have used the model to investigate the role of this channel in electrophysiological signals, such as the action potential and spontaneous transient hyperpolarisations. Furthermore, the clinical effects of BK channel openers, mallotoxin and NS19504, were simulated for the detrusor smooth muscle cells. Our findings support the proposed application of these drugs for amelioration of the condition of overactive bladder. We thus propose a physiologically realistic BK channel model which can be integrated with other biophysical mechanisms such as ion channels, pumps and exchangers to further elucidate its micro-domain interaction with the intracellular calcium environment.

Keywords BK channel · N-shaped I-V curve · Calcium sparks · Action potential · Spontaneous transient hyperpolarisations · Spontaneous transient outward currents · Mallotoxin / Rottlerin · NS19504

Action Editor: Upinder Singh Bhalla

✉ Rohit Manchanda
rmanch@iitb.ac.in

Suranjana Gupta
suranjana.gupta@ieee.org

[1] Computational NeuroPhysiology Lab, Department of Biosciences and Bioengineering, IIT Bombay, Powai, Mumbai- 400076, India

1 Introduction

The large conductance voltage and calcium activated potassium (BK) or Maxi-K channels play a dominant role in governing the excitability of the detrusor smooth muscle (DSM) cells. They modulate the repolarisation and hyperpolarisation phases of the action potential (AP, or spike), in turn controlling the contractile activity of the DSM tissue (Heppner and Bonev 1997; Vergara et al. 1998; Hashitani and Brading 2003; Hashitani et al. 2004;

Hayase et al. 2009; Petkov 2012, 2014). Modulating these channels via drugs may hold promise as a viable option to treat urinary bladder pathologies that might arise from its channelopathies (Turner and Brading 1997; Brading 2006). Studies have shown how alterations in any specific ion channel have affected network functions (Steephen and Manchanda 2009; Mandge and Manchanda 2018). Similarly, mutations in a single BK channel can have profound consequences in an individual cell, which can alter the frequency of signals in a smooth muscle (SM) syncytium, thereby affecting the behaviour of the muscle. Thus, comprehensive insights into the channel's biophysical functioning are required such that its influence on the electrical and contractile activity of the detrusor can be modulated in a targeted manner.

Amongst all known channels, the BK channel has the highest single channel conductance ($100 - 300\ pS$) (Kaczorowski and Garcia 1999; Magleby 2003; Ghatta et al. 2006; Petkov 2012, 2014). BK channels are activated by intracellular calcium concentration ($[Ca^{2+}]_i \triangleq \zeta = 1 - 10\ \mu M$) and membrane voltage (Hristov et al. 2011; Petkov 2012; Engbers et al. 2013; Kyle et al. 2013; Petkov 2014). The channels receive the activating calcium from two different sources (i) ryanodine receptors (RyRs), located on the sarcoplasmic reticulum (SR) membrane and (ii) voltage-dependent calcium channels (VDCCs), present on the plasma membrane (Herrera and Nelson 2002). In order to activate, BK channels require high localised (micro-domain) intracellular calcium concentration in the range $4 - 30\ \mu M$ (Cheng and Lederer 2008). Calcium sparks are the submembrane calcium release events mediated by RyRs, that locally increase the intracellular calcium concentration to $\sim 10 - 100\ \mu M$. Hence, sparks are primarily responsible for the channel's initial activation (Parajuli et al. 2015). Calcium influx through the membrane calcium channels sustains the activation of the BK channel (Hollywood et al. 2000; Herrera and Nelson 2002; Petkov and Nelson 2005; Petkov 2012). In all, therefore, BK channels are activated by three modalities — membrane voltage, calcium influx through the membrane and calcium release from the SR.

Several groups have recorded BK currents under voltage clamp conditions. The studies done so far reported currents with varied temporal characteristics, namely, non-inactivating (Hristov et al. 2011), partially inactivating (Hirano et al. 1998) and completely inactivating (Herrera et al. 2001) current profiles. Similarly, I-V curves with two distinct shapes for the same presumptive channel have been reported, one presenting a profile similar to non-inactivating voltage-gated potassium channels (Meredith et al. 2004, Mahapatra et al. 2018a, b) and the other presenting an 'N-shaped' I-V curve (Meech and Standen 1975; Klöckner and Isenberg 1985). This discrepancy cannot be attributed to variation between animal species as the current recordings from DSM cells of the same species have shown such variability. For example, Hirano et al. (1998) and Herrera et al. (2001) recorded BK currents from DSM cells of guinea-pig, with the former reporting a current with an inactivating profile, and the latter reporting a current with a partially inactivating profile. Similarly, Hristov et al. (2011) reported inactivating and non-inactivating current profiles for BK currents recorded from human DSM cells. A similar inconsistency exists in the case of the BK channel I-V curves (Klöckner and Isenberg 1985; Meredith et al. 2004). However, although varying current and I-V profiles have been reported, it is as yet unclear as to why these differences arise.

The dual activation of BK channels by membrane voltage and intracellular calcium (ζ) is a complex phenomenon as these activation modalities are interdependent on each other. They act synergistically on the channel to activate it (Salkoff et al. 2006; Gupta and Manchanda 2018). In an experimental setup, it is feasible to regulate the membrane potential, such as in voltage clamp studies, but not the intracellular calcium concentration. It is, therefore, experimentally challenging to decode the interdependencies of the underlying intracellular calcium concentration on the one hand and membrane potential on the other.

We felt that a computational model of the BK channel might help shed light on the aforementioned questions, since investigations can be carried out in the computational domain that may not be amenable to experimental exploration. There are several models of BK channels available, of which only a few are smooth muscle specific (Tong et al. 2011; Korogod et al. 2014; Gupta and Manchanda 2014; Kochenov et al. 2015; Mahapatra et al. 2018a, b). BK channels have been primarily modelled using two techniques, i.e., Markov modelling (Moczydlowski and Latorre 1983; Cox et al. 1997; Cox 2014; Mahapatra et al. 2018b) and the Hodgkin-Huxley formalism (Jaffe et al. 2011; Tong et al. 2011; Engbers et al. 2013; Korogod et al. 2014; Gupta and Manchanda 2014; Kochenov et al. 2015; Mahapatra et al. 2018a). Models based on the Markov modelling technique employ several transitional states to describe BK channel activity. Geng and Magleby (2015) and Rothberg and Magleby (2000) predicted a BK channel model with 50 states to completely describe the functioning of the channel. Such models are detailed but computationally highly intensive and time-consuming, rendering them unsuitable for large-scale simulations, such as an integration into a smooth muscle syncytium model (Appukuttan et al. 2015). The smooth muscle specific models based on the Hodgkin-Huxley formalism are computationally less intensive, but fail to reproduce the varied current and I-V profiles reported for this channel because the models focus on currents derived from the individual molecular subunits and not on the channel's activating sources (Tong et al. 2011; Mahapatra et al.

2018a). The channel was previously modelled by employing partial inactivation (see Gupta and Manchanda 2014) in order to reproduce the currents reported for guinea-pig DSM, in Hirano et al. (1998). However, the regulatory subunits present in smooth muscle cells (SMCs) ($\beta 1$) do not confer inactivation (Orio et al. 2006; Salkoff et al. 2006; Petkov 2012, 2014), and the subunits that do confer inactivation ($\beta 2$ and $\beta 3$) are not expressed in smooth muscle cells (Vergara et al. 1998; Lovell et al. 2000; Petkov 2014). Thus, the basic premise that the BK channel partially inactivates is questionable in the case of smooth muscle. It has been conjectured that the BK channel, insofar as its activation by cytosolic calcium is concerned, is activated by two distinct calcium signals; one from the SR (calcium spark) and the other from the membrane calcium channels (Herrera and Nelson 2002). In the light of the aforesaid observations, we hypothesized that the reported variability in current profiles may stem from the activation of the channel by two sources of calcium, and not due to the species-dependent molecular structure of the channel. We, thus, developed a computational model of the BK channel that embodied this property.

The BK channel model proposed here is biophysically constrained, i.e., the model is grounded stringently on available experimental data. Additionally, the model is computationally economical since it employs just two states, the open and closed states, as opposed to the 10 transitional states, reported in Mahapatra et al. (2018b). The BK channel model is based on the Hodgkin-Huxley gating formalism, activated by membrane voltage and by two distinct calcium signals: (i) a signal representing the calcium spark, which is transient, (ii) a signal representing the calcium inflow via membrane calcium channels, which is relatively prolonged. The model was validated against various experimental findings reported by different groups. For instance, we established that the model successfully generated the three distinct BK current profiles, namely the non-inactivating (Hristov et al. 2011), partially inactivating (Hirano et al. 1998) and completely inactivating (Herrera et al. 2001) current profiles. Additionally, the model was able to generate I-V curves typical of non-inactivating voltage-gated potassium channels (Meredith et al. 2004; Mahapatra et al. 2018a, b) and the characteristic 'N-shaped' I-V curves typical of voltage and calcium activated potassium channels (Meech and Standen 1975; Klöckner and Isenberg 1985). The $I - \zeta$ curve also resembled that reported experimentally (Herrera et al. 2001).

Having carried out model validation along these lines, we used our model in order to address questions of the kind that are best posed in the computational domain, viz, (i) testing an existing hypothesis concerning the activation of BK channels by two sources of intracellular calcium, and the absence of inactivation, (ii) using the model to answer open biological questions in relation to the calcium levels required for channel activation, (iii) resolving apparent discrepancies in the experimentally recorded current and I-V profiles of the channel, (iv) simulating electrophysiological signals and gaining insights from the simulations, and (v) employing the model to study the effect of BK channel activators, mallotoxin and NS19504, on the DSM cell. These questions are further adumbrated below.

We first tested the hypothesis that the BK channel is activated by membrane potential and two separate calcium signals; one from the membrane and the other from SR. This hypothesis was first put forth by Herrera and Nelson (2002) and our model endorsed it. With this approach, our model successfully reproduced the various profiles of experimentally recorded currents and I-V profiles mentioned above. Second, an open biological question pertaining to the activation of the channel has been the order of sub-membrane intracellular calcium concentration required by the channel to activate at different membrane potentials, and our model enabled the estimation of this parameter. Along with this, our model predicted the nature of the sub-membrane calcium dynamics underlying the channel's activation under two conditions, i.e., when the cell is at resting membrane potential (rmp) and when the cell is depolarised. Third, our model helped reconcile apparently discrepant observations on the current and I-V profiles of the channel.

Fourth, we employed our model to simulate electrophysiological signals of DSM such as spontaneous transient hyperpolarisations (STHs) and the action potential. STHs have not been simulated prior to this and our model could successfully elicit these transient hyperpolarisations at the resting membrane potential. STHs emerged when BK channels were solely activated by a signal mimicking the calcium spark. Moreover, the BK channel currents underlying these, mimicked the profiles of spontaneous transient outward currents (STOCs). As regards the spike of DSM cells, the BK channel model was found to dominate the repolarisation and hyperpolarisation phases of the AP. Fifth, our model predicts the effect of BK channel openers, mallotoxin and NS19504, on DSM cell excitability. Mallotoxin has found applications in the treatment of hypertension and vasoconstriction disorders (Marx and Zakharov 2004; Zakharov et al. 2005; Maioli et al. 2009), and NS19504 has recently been propounded to alleviate overactivity of the bladder (Nausch et al. 2014). We simulated the effect of these on the DSM spike and from our studies were able to tentatively comment on their proposed clinical testing in the treatment of overactive bladders.

We discuss the implications of these and other findings on aspects of DSM physiology and pathophysiology.

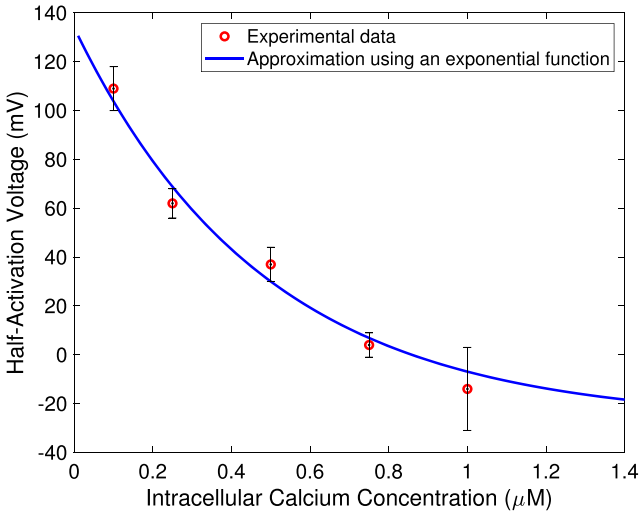

Fig. 1 Plot of the half-activation voltages for different intracellular calcium concentrations

2 Methods

In a previous report (Gupta and Manchanda 2014), the BK channel was modelled using the Hodgkin-Huxley formalism, with four gating particles and partial inactivation. In smooth muscles, BK channels do not inactivate because the regulatory subunits that confer inactivation are absent, as discussed in Section 1. Moreover, assigning gating particles to the channel was ruled out because the activation data obtained from reported experiments pertained to the whole channel, instead of a single particle / unit of the channel.

The model proposed here corrects these former assumptions. In this work, the Hodgkin-Huxley gate model is adapted, where the parameter, m_∞ is a function of both membrane potential and $[Ca^{2+}]_i$ (Hollywood et al. 2000; Zakharov et al. 2005), and the parameter τ_m is solely a function of membrane potential (Herrera et al. 2001; Hristov et al. 2011). The model employs two separate calcium functions, which mimic the inputs from the two calcium sources, RyRs and VDCCs. Figures 1, 2, 3, 4, 5, 6, 7, 8, and 9 were simulated on MATLAB ®(The Mathworks, Inc., Natick, MA) (MATLAB 2018) (R2018a) whereas Figs. 10, 11 and 12 were simulated on NEURON v7.5 (Carnevale and Hines 2006). All simulations were run on a local workstation (8 GB RAM; Intel ®Core™i7-4702MQ).

2.1 Calcium-dependent activation parameters

A simple Boltzmann equation was used to model the activation parameter (1), where the half-activation voltage and the slope factor were functions of intracellular calcium concentration.

$$m_\infty \triangleq \frac{1}{1 + exp\left(-\frac{(V_m - V_{0.5}(\zeta))}{\sigma(\zeta)}\right)} \tag{1}$$

where,

ζ – Intracellular calcium concentration = $[Ca^{2+}]_i$
$V_{0.5}$ – Half-activation voltage
σ – Slope factor
V_m – Membrane potential

In a study by Hollywood et al. (2000), the half-activation voltages and slope factors of BK channels in isolated SMCs of sheep urethra were tabulated. These were compared with the ones reported for vascular tissue, by Zakharov et al. (2005). The half-activation voltages were offset by $> 100\ mV$ but the slope factors in the two studies were in agreement. In Hollywood et al. (2000), the whole channel ($\alpha + \beta 1$ subunits) was present whereas in Zakharov et al. (2005), only the α subunits were present.

It is established that in the presence of β subunits, the activation curve of the channel shifts leftwards i.e., towards hyperpolarised voltages (Kaczorowski and Garcia 1999). $\beta 1$ imparts calcium sensitivity to the channel and this shift in the half-activation voltages (Hollywood et al. 2000) indicate an enhanced sensitivity of the channel to intracellular calcium concentration. However, the slope factor correlates with the number of charged moieties that cross the pore of the channel (Gupta and Manchanda 2018). This suggests that the slope factor depends on the pore-forming subunits alone (the α subunits), which being present in the two studies have resulted in the correspondence of their values.

2.1.1 Half-activation voltage ($V_{0.5}$)

The values documented in Hollywood et al. (2000) were considered for this parameter (Table 1). The data points were approximated using a falling exponential function (2). Most of the $V_{0.5}$ values obtained from the simulation were within the reported experimental range (last column in Table 1: ✓ indicates that the simulated value lies within the range of the experimental data; × indicates that it lies outside the experimental range).

$$V_{0.5} = -27.23783 + \left(161.16921 * e^{-\zeta/0.483}\right) \tag{2}$$

Figure 1 shows the match between the experimentally observed findings and the simulated exponential function. The figure takes into account the error / variation that was reported in Hollywood et al. (2000).

Table 1 Tabulation of experimental (Hollywood et al. 2000) and simulated $V_{0.5}$ values

$\zeta\ (\mu M)$	$V_{0.5\,min}\ (mV)$	$V_{0.5\,avg}\ (mV)$	$V_{0.5\,max}\ (mV)$	$V_{0.5\,simulated}\ (mV)$	$V_{0.5\,min} \leq V_{0.5\,simulated} \leq V_{0.5\,max}$
0.10	100.00	109.00	118.00	103.79	✓
0.25	56.00	62.00	68.00	68.81	×
0.50	30.00	37.00	44.00	30.00	✓
0.75	−1.00	4.00	9.00	6.87	✓
1.00	−31.00	−14.00	3.00	−6.91	✓

2.1.2 Slope factor (σ)

The data reported for this parameter in both Hollywood et al. (2000) and Zakharov et al. (2005), were consistent and thus, combined. The resulting dataset did not exhibit any particular trend because of which its variation could not be approximated by a simple monotonic function. A special three-region TANH spline interpolation technique (Gupta and Manchanda 2014, Eq. 84) was employed to model the slope factor.

$$\begin{aligned}\sigma = {} & 19.5597 + (1.640299 * H) - (4.61883 * (1-H) * \zeta) \\ & -(2.16463 * (1-H) * \eta) + (5.929322 * (1-H) * \eta * \zeta) \\ & +(3.006487 * (1-H) * (1-\eta) * \zeta^2) \\ & +(16.51641 * (1-H) * (1-\eta) * \zeta^3) \end{aligned} \tag{3}$$

where,

$$H = tanh\,(0.1 * (\zeta - 10)) \tag{3a}$$

$$\eta = tanh\,(5 * (\zeta - 0.35)) \tag{3b}$$

The first region was constructed by grouping the data points for concentrations of 20 nM, 0.1 μM, 0.25 μM and 0.5 μM; the second for concentrations of 1 μM and 10 μM and the third region for 100 μM (see Gupta and Manchanda 2014, Table V). The graphical and mathematical variation of the slope factor with intracellular calcium concentration is shown in Fig. 2 and Eq. (3) of this paper, respectively.

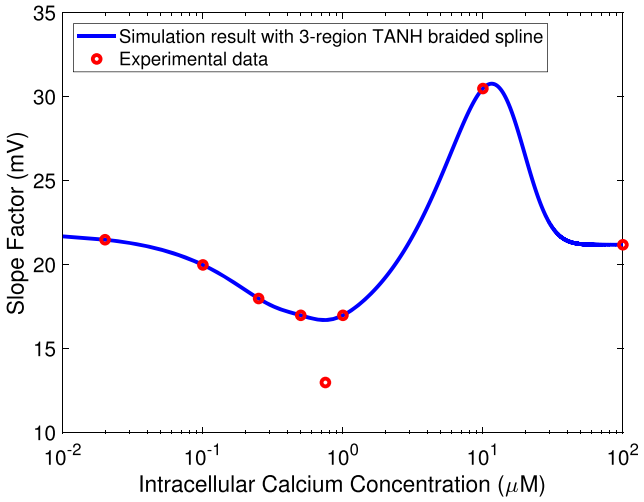

Fig. 2 Plot of slope factor for different intracellular calcium concentrations

2.2 Time constant of activation (τ_m)

BK channels are reported to be activated by the calcium spark, and the activation is sustained by the calcium influx through voltage-gated calcium channels in the membrane (Herrera and Nelson 2002). The current obtained by activation from the spark has been termed the transient BK current and the current evoked by calcium influx via the voltage-gated calcium channels has been termed the steady-state BK current (Herrera and Nelson 2002; Kyle et al. 2013). At the onset of activation, the transient BK current is expressed first, closely followed by the steady-state current. The calcium concentration provided by a spark is sufficient to activate BK channels as the latter require high levels of localised calcium concentration in order to activate (Cheng and Lederer 2008). The stability of the channel-ion complex enables the channel's activation.

In a study by Hristov et al. (2011), the rise times of the transient components of the BK channel currents were tabulated for different clamped membrane potentials. The rise time was stated as the time taken by the current to reach the peak from its baseline value. Using the tabulated rise

Table 2 Tabulation of the rise times, calculated and simulated time constants of activation

$V_m\ (mV)$	$trise\ (ms)$	$\tau_m\ (ms) = \frac{trise}{2.1972}$	$\tau_m(simulated)(ms)$
−40	15.60	7.10	7.26
−20	22.60	10.29	9.88
0	31.90	14.52	14.92
20	40.20	18.30	18.02
40	33.00	15.02	15.14

times, the time constant of activation of the channel was estimated as a function of the membrane potential.

The BK current at a clamped membrane potential of $-40\ mV$ along with an underlying spark, has been reported (see Herrera et al. 2001, Fig. 4B). The rising profile of the BK channel current was best approximated by using an exponential function. The rise time was considered as the time taken for the current to rise from 10% to reach 90% of its peak value instead of (0–100)% of its peak value. Experimentally recorded currents have rounded peaks, which affects the calculation of the time constant if the upper extreme is taken at 100%. Similarly, the presence of noise in experimental currents can impact calculation if the lower extreme is at 0%. Hence, the rise time was chosen to be (10–90)% of its peak value for the calculations (Kobayter et al. 2012).

An exponentially rising current can be approximated using the following (4), where I is the value attained at time t, τ_m is the time constant of rise and I_0 is the peak current attained as $t \rightarrow \infty$.

$$I = I_0 * (1 - e^{-t/\tau_m}) \tag{4}$$

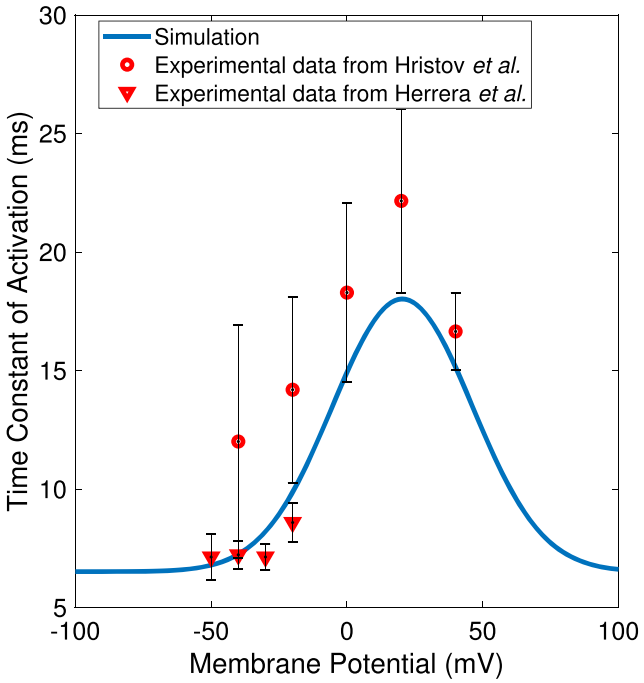

Fig. 3 Plot of the time constant of activation (blue solid line) against membrane potentials. The red circles and triangles indicate the experimental data tabulated in Hristov et al. (2011) and Herrera et al. (2001), respectively

If time taken to reach 10% of the peak value is t_1, and the time taken to reach 90% of the peak is t_2, the following relations hold,

$$0.1 = \left(1 - e^{-t_1/\tau_m}\right) \Rightarrow t_1 = 0.1054 * \tau_m \tag{4a}$$

$$0.9 = \left(1 - e^{-t_2/\tau_m}\right) \Rightarrow t_2 = 2.3026 * \tau_m \tag{4b}$$

$$\text{Rise Time } (trise) = (t_2 - t_1) = 2.1972 * \tau_m \tag{4c}$$

A Gaussian function (5) was used to simulate the variation of the time constant with membrane potential. Table 2 lists the rise times, calculated and simulated time constants of activation. Tables 1 of Herrera et al. (2001) and Hristov et al. (2011) tabulate a range of rise times of the BK current for different clamped membrane potentials. Equation (5) was formulated by considering the minimum values of the rise times reported in Table 1 of Hristov et al. (2011), because it would best represent data from both, Herrera et al. (2001) and Hristov et al. (2011).

$$\tau_m = 6.52717 + \left(11.49647 * e^{\left(-0.5 * \left(\frac{V_m - 20.41929}{25.74647} \right)^2 \right)} \right) \tag{5}$$

Figure 3 plots the simulated time constants of activation as a function of membrane potential. The ranges of experimental values, documented in Herrera et al. (2001) and Hristov et al. (2011) are depicted on the simulated curve. It can be observed that the simulated graph is an optimum fit between the two reported sets of experimental data.

2.3 Intracellular calcium concentration

Based on the hypothesis outlined in Section 1, two different calcium signals were incorporated into the channel model. One signal mimicked the calcium influx from VDCCs (ζ_{ss}) whereas the other mimicked the calcium spark (ζ_t). The intracellular calcium concentration rises rapidly from a baseline value, peaks and then decays gradually to its basal value. Hence, biexponential functions (6) – (11) were chosen to reproduce the time course of the input calcium. These equations differed in the values of the parameters A_s, τ_{fs}, τ_{rs}, R_s, A_t, τ_{ft}, τ_{rt} (see Section 3). A 0.1 μM offset was provided to indicate the basal level of the

cytosolic calcium concentration (Magleby 2003; Gupta and Manchanda 2016).

$$\zeta_{rt}\ (\mu M) = 1 - exp\left(\frac{-t}{\tau_{rt}}\right) \tag{6}$$

$$\zeta_{ft}\ (\mu M) = exp\left(\frac{-t}{\tau_{ft}}\right) \tag{7}$$

$$\zeta_{t}\ (\mu M) = A_t * \zeta_{rt} * \zeta_{ft} \tag{8}$$

$$\zeta_{rs}\ (\mu M) = 1 - R_s * exp\left(\frac{-t}{\tau_{rs}}\right) \tag{9}$$

$$\zeta_{fs}\ (\mu M) = exp\left(\frac{-t}{\tau_{fs}}\right) \tag{10}$$

$$\zeta_{ss}\ (\mu M) = A_s * \zeta_{rs} * \zeta_{fs} \tag{11}$$

where, ζ_{rt} and ζ_{ft} are the rising and falling exponentials governing calcium spark (ζ_t), and ζ_{rs} and ζ_{fs} are the rising and falling exponentials governing the steady-state calcium influx from VDCCs (ζ_{ss}).

2.4 Testing the 'Goodness of Fit'

The R^2 (or adjusted R^2) metric cannot be used as a measure of the goodness of fit for non-linear functions as it strictly applies to linear functions only (Spiess and Neumeyer 2010). In this study, the standard error of regression or the root mean squared error (RMSE) has been chosen to indicate the goodness of fit (Mandge and Manchanda 2018). RMSE is calculated as the square root of the mean squared error.

In the mathematical expression for unbiased RMSE, I_{Exp} is the experimental value, I_{Sim} is the simulated value whose goodness of fit is to be measured, N is the total number of data points and k is the number of parameters, or degrees of freedom (12).

$$RMSE = \sqrt{\frac{\sum(I_{Exp} - I_{Sim})^2}{N - k}} \tag{12}$$

$$Threshold = \frac{RMSE}{max(I_{Sim}) - min(I_{Sim})} * 100 \tag{13}$$

The limitation with the RMSE measure is that there does not exist an absolute range of values that can signify a good, mediocre or a bad fit. Hence, comprehending the goodness of fit with respect to the absolute RMSE values is challenging. Instead of reporting the absolute RMSE values, a 'threshold' parameter is employed (13), which is the ratio of RMSE with respect to the range of simulated data. Threshold tends to acquire a lower value as the fit improves (Mandge and Manchanda 2018).

3 Results

3.1 Activation parameter (m_∞)

The activation parameter, incorporating the half-activation voltage and slope factor (1), (2), (3), was plotted as a function of both membrane potential and $[Ca^{2+}]_i$. It can be seen that m_∞ for the channel is a sigmoidal function of V_m whereas, m_∞ vs $[Ca^{2+}]_i$ rises approximately exponentially for the range of V_m explored (Fig. 4).

Figure 4 suggests the following features of the BK channel behaviour:

i Irrespective of the amount of $[Ca^{2+}]_i$ acting on it, a small fraction of the channels ($< 20\%$) will activate if the voltage is negative to $-60\ mV$, which is the resting membrane potential of detrusor SMCs (Fry et al. 1998; Fry and Wu 1998; Sui et al. 2001).

ii At the resting membrane potential ($\sim -60\ mV$), about 20% of the channels will activate at $\sim 2\ \mu M$ intracellular calcium concentration (see Fig. 4). It is suggested that due to spontaneous openings of the RyRs, BK channels do activate at resting membrane potential and cause spontaneous transient hyperpolarisations (STHs) (Hristov et al. 2011). These STHs hyperpolarise the membrane potential by $\sim 5\ mV$. Thus, a small fraction of BK channels activate when spontaneous calcium sparks are released, which is in accord with Fig. 4.

iii At membrane potentials depolarised to $-60\ mV$, the channel activates even at relatively low $[Ca^{2+}]_i$. The BK channel can half-maximally activate at around $1\ \mu M$ and at voltages above $-20\ mV$. At higher potentials, for the same $[Ca^{2+}]_i$, the channel tends towards

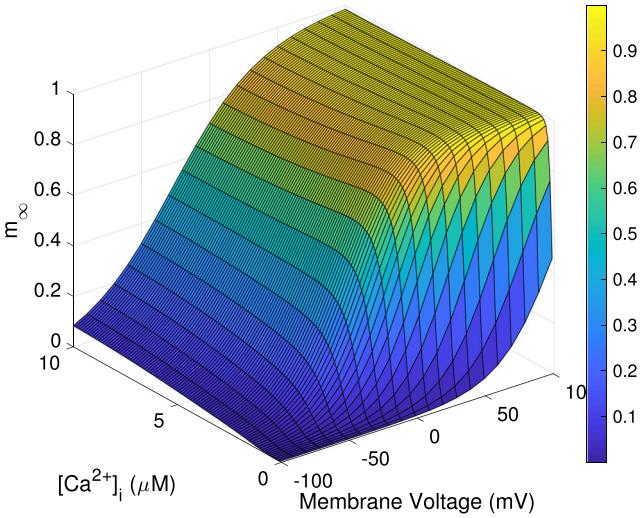

Fig. 4 3D heat map of m_∞ indicating its variation with membrane potential and $[Ca^{2+}]_i$. The extent of activation is indicated by the colour bar alongside the plot

maximal activation. Hence, during an action potential, moderate levels of intracellular calcium concentration may be required for BK channels to activate.

3.2 BK currents and its underlying sub-membrane calcium concentrations

The BK channel model developed here is governed solely by the activation parameters (m_∞ and τ_m), and is devoid of inactivation mechanisms. However, due to two different sources of calcium (6) – (11), two different channel currents are obtained, which represent the transient (Ibk_t) and steady-state (Ibk_{ss}) channel currents, respectively. The overall BK current (Ibk) was obtained by the linear weighted sum of the transient and steady-state currents. The weight given to the transient component (tsr) was 45%, which is in accordance with Herrera and Nelson (2002). The experimental BK currents were obtained from Hirano et al. (1998, Fig. 1Ba).

$$Ibk_{ss} = g_{max} * m(\zeta_{ss}) * (V_m - E_K) \quad (14)$$

$$Ibk_t = g_{max} * m(\zeta_t) * (V_m - E_K) \quad (15)$$

$$Ibk = (tsr * Ibk_t) + ((1 - tsr) * Ibk_{ss}) \quad (16)$$

In order to mimic the experimental traces over a range of different clamp potentials, the parameters of the calcium functions (6) – (11) were tuned. Physiologically, BK channels do not activate instantaneously upon the establishment of the voltage clamp. The voltage-gated calcium channels need to activate first. A calcium influx through these channels activates RyRs, which results in a spark that activates BK channels. Therefore, while simulating these currents, despite the voltage clamp being established at simulation time point $t = 0\ ms$, the calcium signals were provided with an onset delay, in the range $(8 - 10\ ms)$ (Berridge 2008). This was done in order to mimic the physiological delay that emerges due to the activation of VDCCs and RyRs.

Some studies have reported the resting membrane potential of DSM cells to be $-60\ mV$ (Fry et al. 1998; Fry and Wu 1998; Sui et al. 2001), whereas a few others have reported it to be $-50\ mV$ (Klöckner and Isenberg 1985; Hashitani et al. 2004). The Nernst potential of potassium ions (E_K) is about 50% – 80% more negative than the resting membrane potential (Prosser 1974). E_K was assumed to be $-90\ mV$, a value that is 50% more negative than $-60\ mV$ and 80% more negative than $-50\ mV$.

To test the aforementioned hypothesis, the experimental currents from Hirano et al. (1998, Fig. 1Ba) were considered because the current profile seemed to suggest the impact of both RyRs and VDCCs. These partially 'inactivating' currents were recorded from the BK channels in guinea-pig DSM cells. In order to fit the net BK currents to its experimental counterparts, the parameters A_s, τ_{fs}, τ_{rs}, R_s, A_t, τ_{ft}, τ_{rt} and *onset* were tuned so as to obtain the best possible fits (Table 3). By doing so, the model mimicked the experimental currents accurately and was simultaneously able to predict the dynamics of the underlying sub-membrane calcium concentration. Figure 5 demonstrates the simulation results from the model for three clamped potentials. Figure 5Aa, Ba and Ca depict the simulated currents superimposed on the experimental traces, digitized from Hirano et al. (1998, Fig. 1Ba), similar to the approach taken in Gupta and Manchanda (2014). Figure 5Ab, Bb and Cb together constitute a prediction of the sub-membrane calcium concentration that the channel receives during its activation.

The simulated calcium spark lasted for $\sim 200\ ms$, which is in accord with Herrera et al. (2001, Fig. 4B). Under voltage clamp conditions, the influx from VDCCs can be considered steady. Although the simulated calcium influx appears to be at a constant level, it was observed that on increasing the simulation time, the signal decayed back to its basal value in $\sim 6{-}10\ s$, which is around the time span over which a calcium transient has been reported to decay under voltage clamp conditions (Ganitkevich and Isenberg 1991; Dave and Manchanda 2017). Physiologically, the calcium influx from VDCCs will rapidly decay once the clamp is removed. However in the model, in order to hold the biexponential function constant for the duration of the clamp, the respective parameters were so tuned that the function took $\sim 6 - 10\ s$ to decay, which is high for a membrane channel. This could be circumvented by employing a biophysical calcium channel model which has an inherent dependency on the membrane potential. However, this would increase the complexity of the model without a significant gain of accuracy, as the dynamics of the decay phase of VDCCs was not crucial for the results discussed here. The implicit functions (9)–(11) were therefore applied for the analysis. Essentially, Eqs. (6)–(8) mimic a spark, which is a transient phenomenon, and Eqs. (9)–(11) mimic the input from membrane channels which is more prolonged. The latter remains roughly constant during the activation of the BK channel, under voltage clamped conditions.

The following results emerged from our model for BK currents obtained under voltage clamp conditions (Fig. 5):

i The amplitude of the transient BK current was seen to be nearly twice that of the steady-state component at lower potentials. During the onset of the channel's activation, the calcium contributed by the spark is significantly higher than the calcium contributed by membrane channels. In the overall BK current, the

Table 3 The parameters used for the simulation of BK currents and for the goodness of fit

Nernst potential of potassium in bladder smooth muscle (E_K (mV))	−90
Resting membrane potential of bladder smooth muscle (V_{rmp} (mV))	−60
No. of activation particles (mx)	1
The transient-to-steady-state component ratio (tsr)	0.45
Maximum conductance (g_{max}) (nS)	40
Time for which simulation is run (ms)	200
Basal intracellular calcium concentration (μM)	0.1
m_0	0
Number of degrees of freedom (k)	8

V_m (mV)	Onset of Calcium Signals (ms)	Calcium from Membrane (μM)				Calcium Spark (μM)			Threshold	Equivalent $R_{adj.}{}^2$
		R_s	τ_{rs}	τ_{fs}	A_s	τ_{rt}	τ_{ft}	A_t		
40	8	0.80	12	1319	0.64	1	20	1.15	4.611%	0.973
30	8	0.24	3	2221	0.66	8	20	1.70	5.604%	0.961
20	8	0.14	2	1647	0.66	5	19	1.90	5.541%	0.962
10	8	0.15	1	1963	0.66	2	18	2.50	6.097%	0.955
0	8	0.15	13	2316	0.62	4	27	2.00	5.485%	0.963
−10	10	0.20	38	1145	0.58	15	38	2.10	8.176%	0.923

transient component seems to predominate. Across all potentials, it is observed that the spark dominates the calcium influx from VDCCs. This is consistent with the experimental findings which report that BK channels activate through a spark.

ii As the membrane potential is further depolarised, the calcium influx from VDCCs saturates to about $700 - 800\ nM$. However, the calcium from the spark initially increases, peaks to about $2.0\ \mu M$, and then starts diminishing at potentials higher than $10\ mV$. Although ryanodine receptors are not directly influenced by membrane voltages, there appears to be a dependence between the membrane potential and the calcium efflux constituting the spark from these receptors. However, calcium influx from VDCCs appear to stay constant across the different clamped potentials. It is to be emphasized that the calcium traces in Fig. 5Ab, Bb and Cb predict the sub-membrane calcium requirement for BK channel activation. These traces neither illustrate the total output from the receptors and channels, nor the net rise in calcium concentration that occurs in the bulk of the cell. It appears that beyond a particular value of V_m, BK channels require a steady calcium input, $\sim 700 - 800\ nM$ from VDCCs to sustain its activation. According to the I-V curve of VDCCs (Luo and Rudy 1994), the calcium influx from these channels falls beyond a critical membrane voltage. This in turn would simultaneously affect the activation of RyRs. In these simulations, the total calcium acting on the BK channel increases till a particular voltage, beyond which it deteriorates. That critical potential is $10\ mV$, which is in accordance with reported data (Luo and Rudy 1994).

iii Experimentally it has been found that BK channels need $\sim 1 - 10\ \mu M$ $[Ca^{2+}]_i$ for its activation (see Section 1). In Fig. 5, the linear sum of the calcium concentrations comes to a value within this range. It is not possible experimentally to tease out the individual calcium sources when the channel activates. This is because calcium dyes are used to assess the extent of rise of the intracellular calcium concentration. These dyes used in experiments cannot differentiate between calcium that results due to membrane mechanisms and calcium that results due to release from the SR stores.

Figure 5 illustrates the transient, steady-state and overall simulated BK currents superimposed on experimental traces, digitized from Hirano et al. (1998), and the dynamics of the calcium spark, calcium influx from VDCCs, and the total calcium acting on the channel. Although this has been done for all the six clamped potentials (Table 3), only three have been depicted here, i.e. $-10\ mV$, $10\ mV$ and $40\ mV$.

The overall simulated BK current is a non-linear function of time, because of which the RMSE measure (12) has been employed to indicate the goodness of fit. A threshold parameter (13) is reported in Table 3 to indicate the goodness of fit as the absolute RMSE value by itself does not signify whether a fit is good, bad or mediocre (see Section 2). In the case of (adjusted) R^2, a value ≥ 0.95 is considered to be a good fit. In order to quantify our results, we performed a multi-linear regression analysis for the same number of data points and degrees of freedom, as

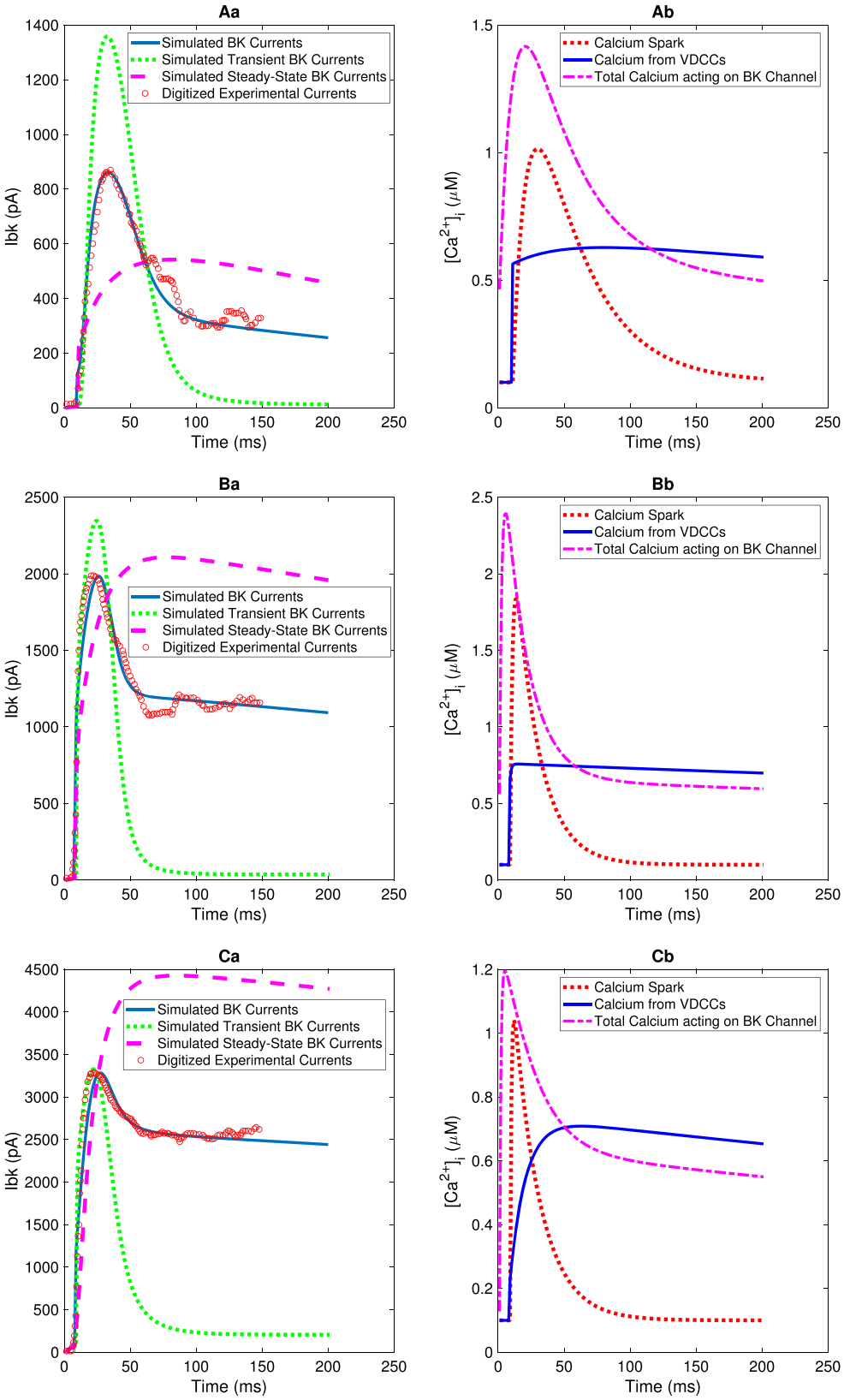

Fig. 5 BK currents and its underlying calcium A: $V_m = -10\ mV$; B: $V_m = 10\ mV$; C: $V_m = 40\ mV$; a: Red circles: Digitized experimental currents from Hirano et al. (1998); Blue solid: Simulated BK currents; Green dotted: Transient BK currents; Magenta dashed: Steady-state BK currents b: Red dotted: Calcium spark; Blue solid: Calcium from voltage-gated calcium channels (VDCCs); Magenta dash-dot: Net calcium concentration acting on BK channel

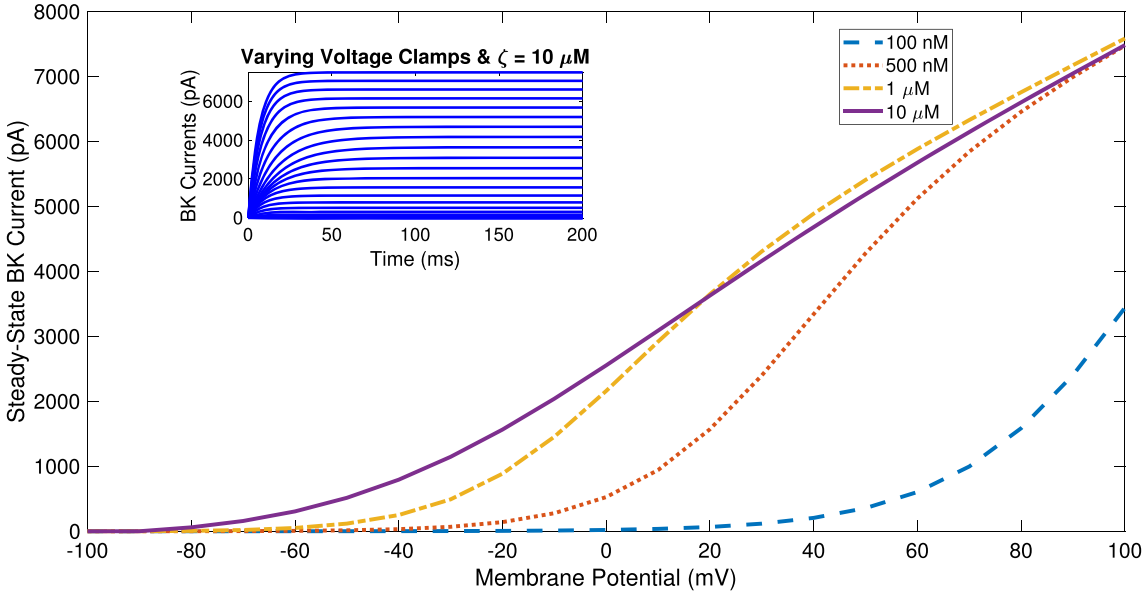

Fig. 6 Steady-state currents vs membrane potential, for different intracellular calcium concentrations held constant. The inset depicts the temporal kinetics of BK currents for different membrane potentials (-100 to $+100\ mV$ in steps of $10\ mV$) and $\zeta = 10\ \mu M$

in these simulations. On this multi-linear data, the adjusted R^2 ($R_{adj.}{}^2$) equivalent for each threshold value (Table 3) was calculated. Through this approach, the goodness of fit corresponding to the threshold values obtained were assessed. The least RMSE score was obtained for $-10\ mV$ and the highest was obtained for $40\ mV$ (Table 3).

The BK currents reported in Hirano et al. (1998) and Herrera et al. (2001, Fig. 4B), for a guinea-pig DSM, reflect partially inactivating and apparent inactivating profiles respectively. Similarly, the BK currents reported in Hristov et al. (2011, Fig. 4A and 5A), for a human DSM, depict non-inactivating and inactivating profiles respectively. As detailed in Section 1, this discrepancy has not been addressed yet. The hypothesis of our study attributes this discrepancy to the underlying activating calcium sources. From Fig. 5 it can be inferred that if BK is co-activated by sparks and voltage-gated channels, a partially inactivating profile results. If BK is activated solely by sparks, an inactivating profile of the current is obtained whereas if BK is activated solely by VDCCs, a non-inactivating profile develops.

3.3 BK channel current–voltage ($I - V$) curve

Figure 6 illustrates the I-V curve of the BK channel for four different intracellular calcium concentrations. These cytosolic calcium concentrations were held constant and BK currents were simulated. The inset in Fig. 6 depicts the BK currents for $\zeta = 10\ \mu M$. The BK currents were simulated over a range of clamped membrane potentials. The steady-state values attained by the BK currents were plotted with respect to its corresponding clamped membrane potential.

The I-V curve mimics the conventional I-V curves of non-inactivating voltage-gated potassium channels. This type of I-V curve has been reported in Meredith et al. (2004), Mahapatra et al. (2018a, b). Thus, if the channel receives a roughly constant calcium concentration during its activation, current profiles and I-V curves similar to those of non-inactivating voltage-gated potassium channels will develop.

Figure 6 permits the following observations:

i At $100\,nM$, which is the basal level of cytosolic calcium (Magleby 2003), BK channels require a large depolarised potential in order to activate.

ii As the intracellular calcium concentration increases, BK channels activate at lower membrane potentials. When $\zeta = 1\,\mu M$, BK channels start activating at $-40\,mV$, which is similar to the condition attained during an AP.

iii When $\zeta = 10\,\mu M$, BK channels are observed to activate at voltages as low as -60 to $-50\,mV$, which is the resting membrane potential for an isolated DSM cell. This finding is in accord with the inferences made for Fig. 4. Thus, for BK channels to activate at the resting membrane potential and induce STHs, it must receive calcium concentrations higher than $1\ \mu M$.

The slope of the I-V curve tends to be steeper with increasing levels of intracellular calcium concentrations. This implies that when the BK channel is driven by

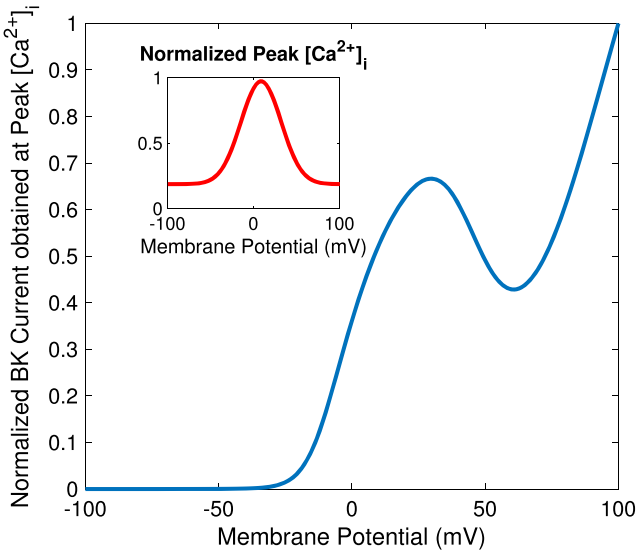

Fig. 7 The characteristic 'N-shaped' I-V curve of BK channels. The inset shows the variation of peak intracellular calcium concentration with respect to the membrane potential. The Gaussian function and the I-V curve are shown normalized

higher cytosolic calcium concentration, a small degree of depolarisation is sufficient to elicit a strong current response from the channel. It is to be noted that in the case of $1\,\mu M$ and $10\,\mu M$, a cross-over is seen at $\sim 20\,mV$, following which the slope of the $1\,\mu M$ plot becomes slightly steeper than that at $10\,\mu M$. It can be concluded that beyond a particular 'threshold' voltage and 'threshold' intracellular calcium concentration, the activation dynamics of BK channels are approximately the same.

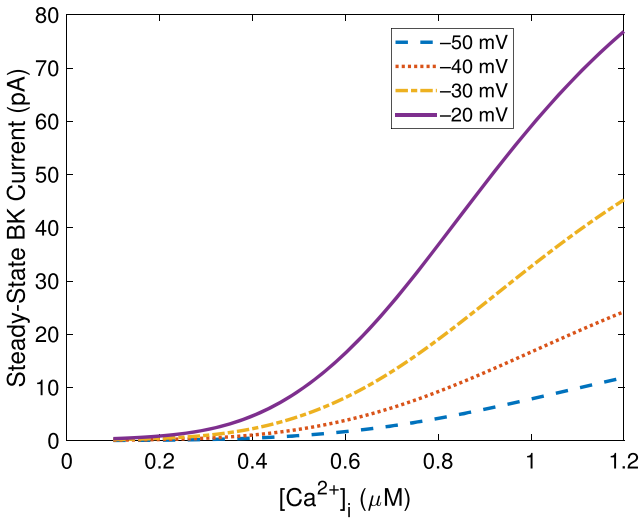

Fig. 8 Steady-state BK currents vs intracellular calcium concentration for different clamp potentials

3.4 The 'N-shaped' current–voltage curve of BK channels

BK channels have been reported to exhibit a characteristic 'N-shaped' I-V curve (Meech and Standen 1975). In the previous section, with calcium concentration levels held constant, this profile of the curve did not arise. As stated before, cytosolic calcium is itself a function of membrane potential and time. Intracellular calcium rises rapidly and decays gradually (Dave and Manchanda 2017) due to which biexponential functions (6)–(11) are used to best approximate this trend of cytosolic calcium in the simulations. However, it has been shown that the peak calcium concentration level attained is also a function of membrane potential (Luo and Rudy 1994, Fig. 5B). This documented variation was best approximated by a Gaussian function (Fig. 7 *inset*). Instead of holding the calcium level constant, the peak of the intracellular calcium concentration was varied using this Gaussian function and the emerging I-V curve was plotted. Figure 7 bears a resemblance to Meech and Standen (1975, Fig. 4B) and Klöckner and Isenberg (1985, Fig. 7B). A better match can be obtained if the exact variation of intracellular calcium with membrane potential is known.

3.5 BK channel current–calcium ($I - \zeta$) curve

BK channels are co-activated by membrane potential and intracellular sub-membrane calcium. The dependency on intracellular calcium was graphically analysed by plotting the $I - \zeta$ curve for a range of clamped membrane potentials. Herrera et al. (2001, Fig. 7) illustrates the BK channel activity with respect to changes in intracellular calcium concentrations for four different membrane potentials. In order to assess the performance of the BK channel model, the same clamped membrane potentials and the same range of intracellular calcium concentrations, as reported in Herrera et al. (2001), were considered. BK currents were simulated and the steady-state values were extracted and

Table 4 List of parameters and their assigned values to simulate STHs

Parameters		Values
Specific membrane capacitance (C_m)		$1\,\mu F/cm^2$
Maximum conductance of BK channel (g_{max})		$40\,nS$
Maximum conductance of Leak channel		$1/138000\ S/cm^2$
Nernst potential of potassium in DSM (E_K)		$-90\,mV$
Reversal potential of the Leak ion channel		$-60\,mV$
Resting membrane potential of DSM (V_{rmp})		$-60\,mV$
Time step (dt)		$1\,ms$
Basal intracellular calcium concentration		$0.1\,\mu M$
Calcium spark parameters	τ_{rt}	$4\,ms$
	τ_{ft}	$27\,ms$

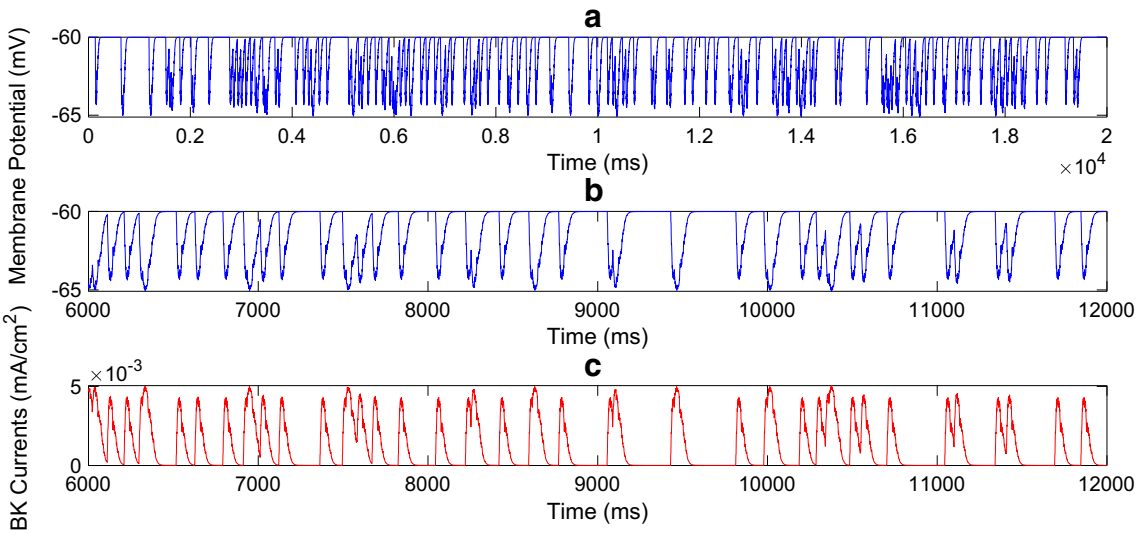

Fig. 9 **a**: Simulating the spontaneous transient hyperpolarisations (STHs) using BK and a non-specific cation (leak) channel; **b**: STHs in (**a**) are expanded to illustrate the kinetics of the membrane potential deflections; **c**: Spontaneous transient outward currents (STOCs) underlying the STHs expanded in (**b**)

divided by the unitary current, which was taken to be 15 pA (Herrera et al. 2001; Hristov et al. 2011). The graph obtained from the model (Fig. 8) resembled the predicted fits made by Herrera et al. (2001, Fig. 7).

3.6 Spontaneous Transient Hyperpolarisations (STHs)

Spontaneously occurring hyperpolarisations have been experimentally recorded in several smooth muscle cells (Jaggar et al. 2000). With the application of iberiotoxin, a BK channel blocker, STHs are supressed suggesting that BK channels underly these signals (Brading 2006; Petkov 2014; Parajuli et al. 2015). It is conjectured that the underlying mechanism for STHs are the spontaneous openings of RyRs that result in focal release of calcium sufficient to activate BK channels at the resting membrane potential (see Figs. 4 and 6). In the present study, we attempted to provide a proof of concept mechanism underlying this phenomenon.

In order to mimic spontaneous openings of RyRs, a train of biexponential functions were employed. The time stamps, extracted from Hristov et al. (2011, Fig. 8A), were used to determine the time at which these simulated sparks would occur. The amplitudes of these simulated sparks were randomly picked from a uniform distribution, and were confined within the physiological range of $1 - 10\ \mu M$. The membrane potential in the model was held constant at its resting value, i.e., $-60\ mV$, and this train of biexponential functions served as the calcium spark input to the BK channel model.

We employed two ion channels to simulate the STHs. Apart from the BK channel, a non-specific cation (leak) channel was included in the simulation. Its reversal potential was set to be equal to the resting membrane potential and its conductance was evaluated by taking the reciprocal of the specific membrane resistance ($= 138\ k\Omega cm^2$) (Fry et al. 1999; Sui et al. 2001) and multiplying it with the surface area of the detrusor smooth muscle cell (length $= 200\ \mu m$; diam $= 6\ \mu m$) (Fry et al. 1999). Hristov et al. (2011, Fig. 8A) depicted the maximum hyperpolarising potential of the STHs to be $\sim 5\ mV$. Certain parameters were tuned in order to obtain membrane potential deflections that lay within this experimentally recorded range. The parameters used for this simulation are listed in Table 4.

As described above, transient hyperpolarisations punctuating the rmp resulted when our BK channel model was activated. The hyperpolarisations are plotted in Fig. 9a. A portion of the figure has been expanded in Fig. 9b to display in greater detail the kinetics of the deflections in membrane potential. The model simulated random firing to emulate the stochastic openings of the RyR clusters. However, because calcium sparks are transient in nature, BK channels stay activated for only a short duration. The activation and deactivation of these channels result in spontaneous transient outward currents (STOCs) (Bolton and Imaizumi 1996; Fry et al. 1998; Parajuli et al. 2016), shown expanded in Fig. 9c. These currents produce momentary and spontaneous hyperpolarising deflections from the resting value of the membrane potential, similar to the experimental traces in Hristov et al. (2011).

Table 5 Parameters used for the simulation of the single-cell action potential (the remaining parameters can be obtained from their respective original models, mentioned in the text)

Parameters	Values	References
Single Cell		
Resting membrane potential	$-60\ mV$	Fry et al. (1998), Fry and Wu (1998), and Sui et al. (2001)
No. of segments (nseg)	1	
Length of DSM cell	$200\ \mu m$	Fry et al. (1999)
Diameter of DSM cell	$6\ \mu m$	Fry et al. (1999)
Specific cytoplasmic resistance	$183\ \Omega cm$	Fry et al. (1999)
Specific membrane capacitance	$1\ \mu F/cm^2$	Sui et al. (2001)
Specific membrane resistance	$138\ k\Omega cm^2$	Fry et al. (1999) and Sui et al. (2001)
Reversal potential of leak channel in the DSM cell	$-60\ mV$	
Basal calcium concentration	$150\ nM$	Dave and Manchanda (2017)
Diffusion co-efficient of calcium	$0.6\ \mu m^2/ms$	Donahue and Abercrombie (1987) and Mandge and Manchanda (2018)
Duration for which simulation is run (Tstop)	$1800\ ms$	
Time step (dt)	$0.025\ ms$	Carnevale and Hines (2006)
Synaptic Input		
tau1	$5\ ms$	Tuned
tau2	$30\ ms$	Tuned
gmax	$0.02\ \mu S$	Tuned
Ion channels		
BK channel conductance (g_{max})	$0.00032\ S/cm^2$	
Transient-to-steady-state ratio (BK) (tsr)	0	
SK channel conductance	$0.00001\ S/cm^2$	Tuned
IK channel conductance	$0.008\ S/cm^2$	McDougal et al. (2017, ModelDB accession number 243842)
KATP channel conductance	$0.0001\ S/cm^2$	Tuned
KCNQ channel conductance	$0.0009\ S/cm^2$	Tuned
KDR channel conductance	$0.0001\ S/cm^2$	Tuned
Nernst potential of potassium in the DSM cell (E_K)	$-90\ mV$	Prosser (1974)
L-type calcium channel conductance	$0.00033\ S/cm^2$	Tuned
T-type calcium channel conductance	$0.0002\ S/cm^2$	McDougal et al. (2017, ModelDB accession number 243842)
Nernst potential of calcium in the DSM cell (E_{Ca})	$120\ mV$	Cheng and Lederer (2008)
IH channel conductance	$0.00001\ S/cm^2$	Tuned
Reversal potential of IH channel in the DSM cell	$-29\ mV$	McDougal et al. (2017, ModelDB accession number 243842)
Calcium dynamics		
Fast buffer concentration (B1)	$6\ mM$	Tuned
Forward rate constant of B1	$100\ /mM - ms$	Dave and Manchanda (2017)
Backward rate constant of B1	$50\ /ms$	Tuned
Diffusion co-efficient of B1	$0.1\ \mu m^2/ms$	Personal Communication
Slow buffer concentration (B2)	$5\ mM$	Tuned
Forward rate constant of B2	$0.05\ /mM - ms$	Dave and Manchanda (2017)
Backward rate constant of B2	$2 * 10^{-5}\ /ms$	Dave and Manchanda (2017)
Maximum velocity of PMCA pump	$3.2 * 10^{-17}\ mol/cm^2 - ms$	Dave and Manchanda (2017)
Dissociation constant of PMCA pump	$200\ nM$	Dave and Manchanda (2017)
Maximum velocity of SERCA pump	$3.5 * 10^{-16}\ mol/cm^2 - ms$	Dave and Manchanda (2017)
Dissociation constant of SERCA pump	$219\ nM$	Dave and Manchanda (2017)
Volume of cytosol in DSM cell	85%	Bygrave and Benedetti (1996)

3.7 Effects of BK channel on a single-cell action potential

In order to study the impact of the BK channel model on a DSM action potential, we integrated this channel with other DSM-specific ion channel models. The composite model comprised voltage dependent calcium channels (VDCCs), namely the L- and T-type calcium channels, delayed rectifier (KDR), and Kv7.2 (KCNQ) voltage-gated potassium channels, hyperpolarisation activated non-selective cation channel (IH), intermediate conductance calcium-activated potassium (IK) channel, ATP-activated potassium (KATP) channel and leak channel, sourced from Mahapatra et al. (2018b) and the small conductance calcium-activated potassium (SK) channel from Gupta and Manchanda (2016). Additionally, a detailed DSM-specific calcium dynamics model was adapted from Dave and Manchanda (2017), which comprised models for the sodium-calcium exchanger (NCX), plasma membrane calcium ATPase (PMCA) and sarcoplasmic endoplasmic reticulum calcium ATPase (SERCA) pumps, calcium release from sarcoplasmic reticulum, fast mobile (B1) and slow immobile (B2) buffers. The calcium dynamics model also incorporated the mechanism of radial diffusion of intracellular calcium within the cell, due to which the calcium concentrations at varying radial distances from the plasma membrane (*Shells*) could be assessed (Dave and Manchanda 2017). The robustness of the integrated model was tested by varying each of the ion channel's conductance by $\pm 20\%$ of its control value (Mijailovich et al. 2017). A stable response was observed for each of these conditions (not shown).

Table 5 lists important parameters of the composite model, some of whose values were tuned with respect to the original models (Gupta and Manchanda 2016; Dave and Manchanda 2017; McDougal et al. 2017, ModelDB accession number 243842). The entire model was integrated and tested on the NEURON v7.5 simulation platform (Carnevale and Hines 2006).

Instead of using a current clamp stimulus, a biophysically relevant synaptic input was employed to elicit an action potential (Fig. 10a). This was done because the synaptic input closely mimicked the action of neurotransmitters on the smooth muscle. The DSM-specific ion channel models (McDougal et al. 2017, ModelDB accession number 243842) were normalized with respect to the body temperature. Thus, a temperature correction factor (q10) of 2.3 was chosen to bring the parameters of our BK (and SK) channel models to a body temperature of 37°C. A large onset time for the input stimulus (1000 ms), was provided in order to stabilize the resting membrane potential of this highly non-linear dynamic system.

BK channels are activated by sub-membrane calcium concentrations, as RyR-BK co-localisation occur at a small depth of $20-600\ nm$ below the plasma membrane (Lifshitz et al. 2011; Parajuli et al. 2016). In order to comply with this, the BK model was made to read the calcium concentration in *Shell* 0, which is at a depth of $0.1\ \mu m$ (Dave and Manchanda 2017) from the plasma membrane (Bolton and Imaizumi 1996). The calcium influx through VDCCs and calcium released by SR, together contributes to the rising phases of the calcium transients in all *shells*, due to which the transient-to-steady-state ratio for BK channel was maintained at 0. IK and SK channels are known to be activated by much lower calcium concentrations which arises due to their spatial distances from VDCCs and RyRs. However, this detailed calcium dynamics model (Dave and Manchanda 2017) lacked the mechanism of longitudinal diffusion. As a result of this, the IK and the SK channels were artificially made to read calcium concentrations from a lower *shell* (*Shell* 5) than that read by the BK channel model.

The buffer parameters in Dave and Manchanda (2017) were tuned such that the dynamics of intracellular calcium conform with known properties of sub-membrane calcium dynamics. According to the model parameters employed in Dave and Manchanda (2017), the calcium concentrations were restored to their basal values after several seconds (see Dave and Manchanda 2017, Fig. 3). Although this may be valid for calcium transients arising in the bulk of the cell, we assume that the decay kinetics of sub-membrane calcium transients would be much faster, like a calcium spark. This assumption is well-founded because if the sub-membrane calcium transient persisted for several seconds, the restoration to rmp after an AP would also take the same time as the calcium activated potassium channels would hyperpolarise the membrane potential for as long as the transient persisted. Thus, in the current model, we modified the buffer parameters so that the sub-membrane calcium transient, which is driving the BK channel, decays as rapidly as sparks do.

It was observed that after eliciting the AP, the rmp stabilised in about 4000 ms. However, in order to emphasize the characteristics of the AP and its underlying currents, the respective figures have been depicted over the interval $800-1500\ ms$. The effect of BK channel was assessed by observing the changes in the AP parameters resulting from 'blocking' the channel to various degrees. The rmp, maximum and minimum potentials of the AP were observed to vary almost linearly when the channels' conductance was gradually reduced. Complete blocking of the BK channel was induced by setting the channel's conductance to zero. Following complete block, the amplitude and width of the action potential were markedly enhanced, whereas there was a negligible change in the resting membrane potential (Fig. 10a). Blocking BK channels eliminated the hyperpolarisation phase, and an after-depolarisation phase (ADP)

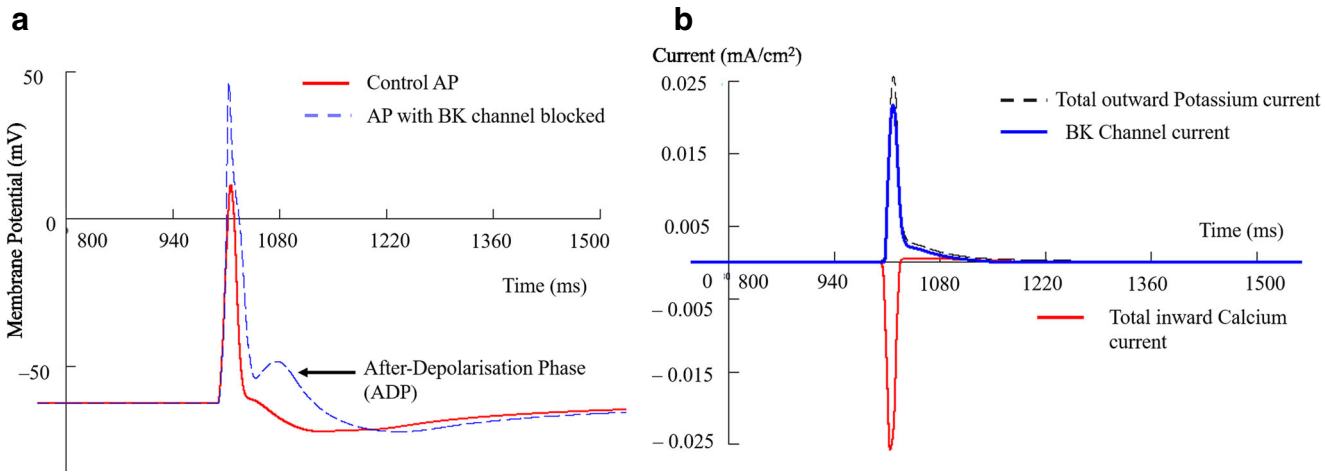

Fig. 10 **a**: Simulated action potentials; Red solid trace: Control action potential; Blue dashed trace: The effect of blocking BK channels **b**: Currents underlying the control AP; Red solid negative trace: Total inward current carried by calcium ions; Black dashed positive trace: Total outward current carried by potassium ions; Blue solid positive trace: BK currents

surfaced (Fig. 10a), substantiating the role of BK channels in the hyperpolarisation phase of the action potential. The simulated effects of BK channel on an action potential were quantified and compared with the experimental findings reported in Table 1 of Hayase et al. (2009). This comparison is documented in Table 6 of this paper.

Given the marked effect of BK channel block on AP parameters, we examined the total inward, outward and BK channel currents (Fig. 10b) underlying the action potential. The BK current constitutes 80.46% of the total outward current (Table 7). This is in agreement with experimental findings which report that BK channels play a dominant role in the repolarisation and hyperpolarisation phases of the action potential (Petkov 2012; Kyle et al. 2013; Petkov 2014).

3.8 Mimicking the action of Rottlerin/Mallotoxin (MTX)

Apart from being heavily modulated by cytosolic calcium, BK channels are also controlled by membrane potential. It has been reported that depolarised membrane potentials increase the sensitivity of the BK channel to cytosolic calcium concentration (Rothberg and Magleby 2000). Thus, in the absence of cytosolic calcium, the channel can still activate but requires much higher activation voltages (Fig. 4).

Mallotoxin (or rottlerin) is a drug that has been propounded for the treatment of hypertension and vasoconstriction disorders (Marx and Zakharov 2004; Maioli et al. 2009). Mallotoxin reduces the dependency of the BK channel on cytosolic calcium concentration and shifts the activation curve of the channel by 100 mV towards hyperpolarising potentials (Zakharov et al. 2005; Guan et al. 2017). Thus, under the influence of mallotoxin, the BK channel activates in the absence of a rise in calcium concentration and behaves like a voltage-gated potassium channel.

In order to simulate the effect of mallotoxin on DSM cells, the half-activation voltage of the BK channel was left-shifted by 100 mV, i.e., towards hyperpolarising potentials. The intracellular calcium concentration driving the BK channel was lowered to nanomolar levels. Under this condition, an AP was elicited as shown in Fig. 11a

Table 6 Simulated effects of BK channel on AP parameters, compared with experimental data (Hayase et al. 2009)

	Simulation			Hayase et al. (2009)	
	Control	100% BK Block	Difference (Control–Block)	Deviation between 'Control' and '100nM IbTX'	Are simulation values within experimental limits?
rmp (mV)	−62.92	−62.84	−0.08	(−4.6) to (+5.4)	✓
Peak Amplitude (mV)	11.44	46.59	−35.16	Not Documented	NA
Magnitude (mV)	74.35	109.43	−35.08	(−16.6) to (+0.2)	×
Half-duration (ms)	16.24	20.16	−3.92	(−4.8) to (+0.4)	✓
$R.dV/dt_{max}$ (mV/ms)	4.39	7.72	−3.33	(−6.2) to (+3.2)	✓
$F.dV/dt_{max}$ (mV/ms)	−0.71	−0.54	−0.17	(−7.5) to (+2.5)	✓

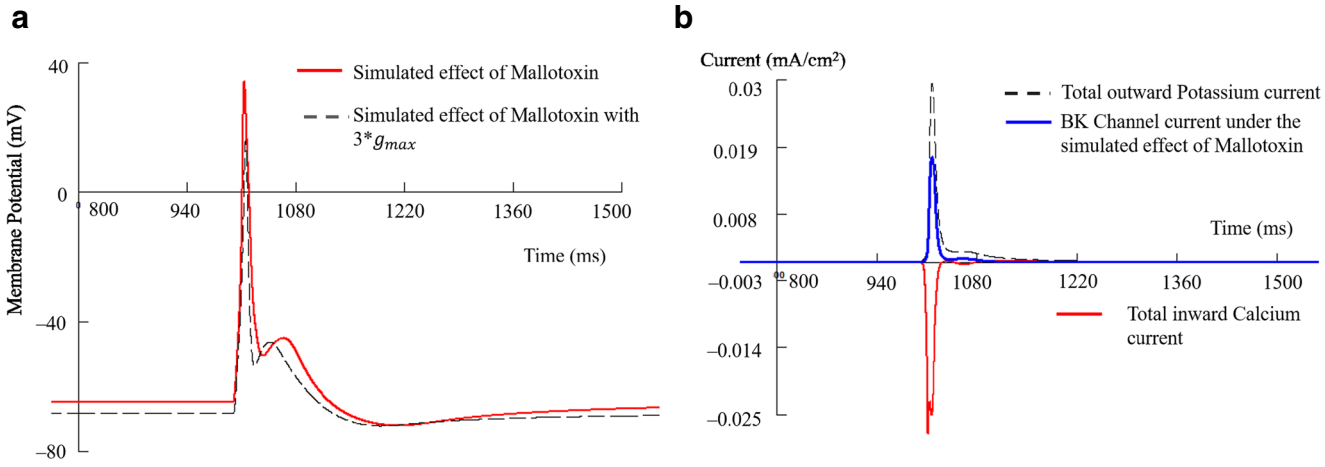

Fig. 11 **a**: Action potential elicited by mimicking the action of the drug mallotoxin; Red solid trace: AP generated without a change in BK channel conductance (AP_{MTX}); Black dashed trace: AP_{MTX} elicited with BK channel conductance increased to three times its control value **b**: Current traces underlying AP_{MTX}; Blue solid positive trace: BK currents; Red solid negative trace: Total inward current carried by calcium ions; Black dashed positive trace: Total outward current carried by potassium ions

(AP_{MTX}). The AP and BK current parameters obtained under the simulated influence of mallotoxin were compared with the control AP (Fig. 10a), and documented in Table 7. Figure 11b plots the total inward, outward and BK channel currents underlying AP_{MTX}. Despite negligible calcium concentration, the BK channel contributed to 44.92% of the total outward current. However, it must be noted that under the influence of mallotoxin, the AP generated had a much larger amplitude, as compared to the control AP (Table 7), and a prominent ADP phase. Additionally, the contribution of BK channels to the outward current was reduced from 80.46% to 44.92%.

It is a widely accepted finding that during pathological conditions, various compensatory mechanisms surface, such as under- or overexpression of channels. For instance, the activation curve of a VDCC shifts leftward in an unstable bladder (Fry and Wu 1998), which could in turn alter the expression profiles of other ion channels in the DSM cell. In this study, the effect of mallotoxin in the presence of overexpressed BK channels was additionally investigated. Under the simulated exposure to mallotoxin, the BK channel conductance was increased to 3 times its control value. The parameters of the AP, elicited under this condition were compared with the control AP (Fig. 10a) and with AP_{MTX} (Fig. 11a). With the BK channel conductance increased to 3 times its original value, the AP elicited had parameters in the range of those obtained for the control AP (Fig. 10a), as has been documented in Table 7. The contribution of BK channels to the outward current increased from 44.92% to 69.95%.

Despite these similarities in the AP parameters, one noticeable difference between the control AP and AP_{MTX} was the presence of the hyperpolarising phase in the control AP (Fig. 10a). The sole difference between the conditions for Figs. 10 and 11 is the level of intracellular calcium concentration acting on the BK channel, which was negligible in the latter. This indicates that if the cytosolic calcium in the cell is low, then despite increases in BK channel expression or conductance, the hyperpolarising phase of the AP will be absent.

Table 7 Comparison of AP and BK current parameters between control AP, AP elicited under the influence of mallotoxin and unchanged BK conductance, and AP elicited under the influence of mallotoxin and increased BK channel conductance

	Action Potential Parameters					BK Current Parameters	
	rmp (mV)	Peak amplitude (mV)	Half-duration (ms)	$R.dV/dt_{max}$ (mV/ms)	$F.dV/dt_{max}$ (mV/ms)	Magnitude mA/cm^2	% of outward current
Control	−62.92	11.44	16.24	4.39	−0.71	0.0217	80.46
Mallotoxin	−64.82	34.13	12.00	6.90	−0.54	0.0172	44.92
Mallotoxin + 3 ∗ g_{max}	−68.12	15.82	9.20	5.42	−0.51	0.0299	69.95

3.9 Effect of BK channel activation in a pathologically overactive DSM cell

NS19504 is a BK channel activator which has been suggested to ameliorate spontaneous contractions in the bladder smooth muscle (Nausch et al. 2014). This compound acts on the channel and, similar to mallotoxin, shifts the half-activation voltage of the channel by 60 mV towards hyperpolarised potentials. In this study, we simulated an overactive DSM cell and observed the effect of NS19504 on it.

The cell was made hyperexcitable by increasing the IH channels' conductance to 0.0009 S/cm^2. The input stimulus was eliminated so that spontaneous APs could be generated. In order to study the effect of the BK activator NS19504, the BK conductance was reduced to 0. Under these conditions, spontaneous APs were elicited within the first 500 ms of the simulation (Fig. 12). The effect of NS19504 was simulated solely by restoring the BK channel's conductance to its control value (Table 5), and left-shifting the half-activation voltage by 60 mV. A stable rmp was obtained and spontaneous APs were eliminated (Fig. 12).

4 Discussion

BK channels are widely expressed in electrically excitable cells such as neurons and muscle cells, and in non-excitable cells, where they are suggested to influence a variety of physiological phenomena. In non-excitable cells, such as cochlear hair cells, these channels regulate signal transduction pathways (Kaczorowski and Garcia 1999; Ghatta et al. 2006). When expressed in electrically excitable SMCs, such as those of trachea, arteries, colon, uterus and bladder, they mediate calibration of electrical excitability by regulating the repolarisation and hyperpolarisation phases of the action potential (Salkoff et al. 2006; Petkov 2012; 2014). BK channels play an important role by acting as a transducing element between the action potential and the calcium transient. The calcium transients in turn govern the contraction profile of the cell (Hashitani et al. 2004). Thus, BK channels are of paramount importance as they participate in controlling the contractility of smooth muscle cells.

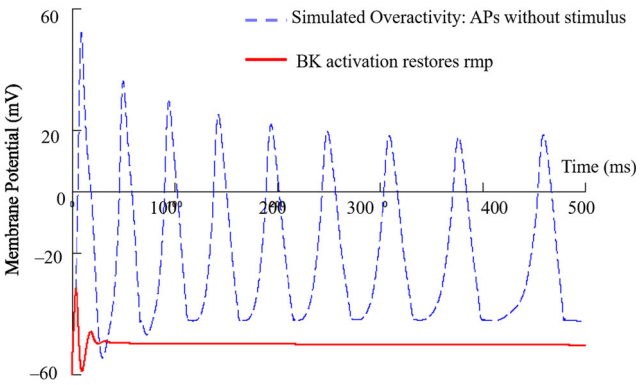

Fig. 12 Simulating the effect of NS19504 on an artificially induced overactive DSM cell; Blue dashed lines: Spontaneously generated APs; Red solid line: Stabilization of rmp due to the effect of NS19504

Below, we discuss (i) Model development and validation; (ii) Comparison of our proposed model with other existing BK channel models; (iii) Implications for BK channel and calcium sources; (iv) Implications for DSM electrophysiology and contractility, and (v) Limitations and avenues for further exploration.

Model development and validation A model of the BK channel has been created using the Hodgkin-Huxley gate formalism, whose parameters were mathematically formulated from reported experimental findings (Section 2). By inspecting the graphical dependence of m_∞ with respect to V_m and $[Ca^{2+}]_i$ (Fig. 4), the activation mechanism of the channel, both at rest and during the action potential, was further elucidated. As outlined in Section 1, BK channels expressed in DSM have been reported to show widely differing current profiles (Hirano et al. 1998; Herrera et al. 2001; Hristov et al. 2011) as well as I-V characteristics (Meech and Standen 1975; Klöckner and Isenberg 1985; Meredith et al. 2004; Mahapatra et al. 2018a, b). The driving hypothesis of this study is that this variability stems from the activation of the channel by two distinct calcium sources, i.e., calcium from RyRs on the SR membrane and from VDCCs on the cell surface membrane (Herrera and Nelson 2002). Our model was successfully able to generate the different current and I-V profiles. Additionally, the model was able to reproduce the characteristic 'N-shaped' I-V curves and $I - \zeta$ curves.

Comparison of our proposed model with other existing BK channel models We compared the performance of our BK channel model with those available in the literature (Moczydlowski and Latorre 1983; Rothberg and Magleby 2000; Tong et al. 2011; Korogod et al. 2014; Kochenov et al. 2015; Mahapatra et al. 2018a, b), and found our model to be superior in performance to the others (Table 8). For any smooth muscle BK channel to be deemed acceptable, it should satisfy the following criteria:

i Should be able to reproduce the inactivating, non-inactivating and partially inactivating BK current profiles,
ii Should be able to mimic the disparate I-V profiles, which include the conventional I-V curve typical of non-inactivating voltage-gated potassium channels and the 'N-shaped' I-V curve characteristic of BK channels,

iii Should be able to generate the $I - \zeta$ curve, and
iv Should support occurrence of spontaneous transient hyperpolarisations (STHs) which is possible if the channel is able to activate at the resting membrane potential and physiological levels of calcium concentrations i.e, $(1 - 10)\ \mu M$.

In Table 8 we summarise the performance indices in relation to each of the models surveyed. Among the models, the DSM-specific BK channel reported by Korogod et al. (2014) could not reproduce the conventional I-V curve typical of non-inactivating voltage-gated potassium channels. The DSM-specific BK channel reported in Mahapatra et al. (2018a, b) and the skeletal muscle based BK channel reported in Moczydlowski and Latorre (1983, Scheme III) could not reproduce the disparate BK current profiles. Although uterine smooth-muscle-specific Tong et al. (2011) and DSM-specific Kochenov et al. (2015) could successfully reproduce the disparate BK current profiles and the conventional I-V curve of non-inactivating voltage-gated potassium channels, Tong et al. (2011) could not mimic the $I - \zeta$ curve whereas Kochenov et al. (2015) could not reproduce the N-shaped I-V curve, which is characteristic of the BK channel. Further, the model proposed by Rothberg and Magleby (2000, Fig. 2D) did not support the occurrence of spontaneous transient hyperpolarisations as the channel model required calcium concentrations of the order of a few hundred micromolar to activate at the resting membrane potential.

Additionally, a simplified equivalent of the 50-state model comprising of 25 states (Rothberg and Magleby 2000) was compared with our proposed BK channel model. Under a clamped membrane potential of 30 mV and steady calcium concentration ($\zeta = 5.5\ \mu M$), the open probability and the activation parameters for Rothberg and Magleby (2000) and our proposed model, respectively, were computed iteratively 72000 times. While the execution time of our proposed BK channel model was 53.22 ms, the same for the 25-state model was 4.50 s, i.e., around 85 times longer. To further elucidate the impact of a model with lower computational intensity, the execution time of the 25-state model was compared with our NEURON-based integrated model for the action potential, which combined 10 ion channel mechanisms, 2 pumps and buffer mechanisms, an exchanger model, calcium release from SR and radial diffusion mechanisms, each of which is complex and non-linear and results in a highly dynamic model. The integrated model was run on the same system (see Section 2), for the same number of iterations, (Table 5: dt = 0.025 ms; Tstop = 1800 ms) as the 25-state model and our proposed BK channel model. The execution time of this complex and non-linear dynamic NEURON - based integrated model for the action potential was just 10.55 s, i.e., around 2.3 times more than the time taken by the 25-state BK channel model alone. This finding reinforces our contention that our proposed model, while being accurate in its predictions, is also greatly less intensive computationally, which makes it more amenable for incorporation in large-scale network simulations.

Implications for BK channel and calcium sources Our simulations demonstrate that when cytosolic calcium is derived solely from RyRs, the BK channel yields a current that has an inactivating profile of the type reported earlier (Herrera et al. 2001; Hristov et al. 2011), and when calcium influx solely from VDCCs acts on the channel, non-inactivating currents (Hristov et al. 2011) are obtained. In this scenario, the partially inactivating current profile (Hirano et al. 1998) can be regarded as a result of calcium inputs via co-activation of RyRs and VDCCs. Our contention is amenable to being experimentally tested, for example by administering selective VDCC and RyR blockers, such as nifedipine (Hashitani and Brading 2003; Kobayter et al. 2012) and ruthenium red (Hirano et al. 1998), and recording the resulting BK currents. Our study explored the differences in the model's responses when either of the two calcium inputs were missing and correlated these differences with reported experimental findings. Thus, our model corroborates existing theories on RyR-VDCC co-activation (Herrera and Nelson 2002) and demonstrates how this co-activation produces the variation in the channel behaviour.

Likewise, I-V curves similar to non-inactivating voltage-gated potassium channels could be obtained when intracellular calcium received by BK channel is held constant. In contrast, an 'N-shaped' I-V curve was obtained when intracellular calcium concentration varied with membrane potential. The calcium influx from VDCCs was seen to be roughly constant under voltage clamp conditions, whereas the calcium spark amplitude varied with membrane potential. Coupling between RyRs and SR membrane potential has been studied in skeletal and cardiac cells which indicated a voltage dependency in the receptor (Laver and Lamb 1998). However, the interaction between RyRs and the plasma membrane potential for smooth muscle cells is yet to be investigated. At present, although we cannot precisely demarcate the exact mechanisms that yield the two I-V profiles in smooth muscle, it is possible to conjecture the conditions under which they may be obtained. Thus, our model has been able to resolve the disparity in current and I-V profiles and unify the apparently conflicting experimental observations by employing two sources of calcium in addition to membrane voltage as the activating signals to the BK channel.

The model was used to answer open biological questions such as the concentration of intracellular calcium required to activate the channel over a range of membrane potentials.

Table 8 Comparative study of performance indices between existing muscle-specific BK channel models and our proposed BK channel model. — indicates not tested, ✓ indicates the successful replication of the experimental traces or curves, × depicts results at variance with experimental observations. Note that whereas each other model fails to satisfy one or more criteria, our model proposed here fulfils them all

Citation	Model Source Code	Type of Muscle Cell	BK Currents	I-V curve	N-shaped I-V curve	$I-\zeta$ curve	STHs
Tong et al. (2011)	Built & Verified	Uterine SM	✓	✓	✓	×	–
Korogod et al. (2014)	Built	Detrusor SM	–	×	–	–	✓
Kochenov et al. (2015)	Built	Detrusor SM	✓	✓	×	✓	–
Mahapatra et al. (2018b)	ModelDB Accession: 243842	Detrusor SM	×	✓	–	×	–
Moczydlowski and Latorre (1983)	ModelDB Accession: 3509	Rat Skeletal	×	×	×	×	×
Rothberg and Magleby (2000)	Built (Fig. 2D & Eq. (4))	Rat Skeletal (Cultured)	–	–	–	–	×
Mahapatra et al. (2018a)	Provided by authors	Detrusor SM	×	✓	×	×	–
Present study	ModelDB Accession : 253490	Detrusor SM	✓	✓	✓	✓	✓

Our model helps speculate on the regions of membrane voltage over which membrane calcium channels and the RyRs dominate in their influence on the activation of the BK channel, thereby providing an insight into the sub-membrane calcium dynamics that underlie the channel's activation. It attempts to provide an insight into the complex interdependencies between membrane voltage and sub-membrane calcium dynamics, which is hard to study experimentally as these signals are coupled to each other physiologically.

Implications for DSM electrophysiology and contractility

Our simulations of electrophysiological signals, such as APs and STHs, observed at the cellular level afford interesting insights into the behaviour of the DSM cell. BK channels do not have a dominant effect on the resting membrane potential (Hayase et al. 2009; Petkov 2012, 2014), a finding that this study was able to corroborate (Table 6). For BK channels to activate at the resting potential, the intracellular calcium levels must be much higher than at rest (see Fig. 4). It is known that RyR activation produces calcium concentrations of the order of $10-100\ \mu M$ at spatial focal points of release (Jaggar et al. 2000; Cheng and Lederer 2008). Therefore, for BK channels to activate at the resting membrane potential, RyRs need to activate first. Co-localisation of RyRs and BK channels enables activation of the latter resulting in the formation of spontaneous transient outward currents (STOCs) (Bolton and Imaizumi 1996; Fry et al. 1998; Jaggar et al. 2000). These currents in turn hyperpolarise the resting membrane potential, thereby generating spontaneous transient hyperpolarisations (Hristov et al. 2011). We simulated STHs by providing a train of biexponential functions that mimicked the spontaneous openings of RyRs (Fig. 9). The mechanism underlying the generation of spontaneous calcium sparks is unknown but further insight is possible if the BK channel is integrated with a model of RyR such that the STHs emerge from an interaction between the two models.

To explore the effects of the BK currents on the action potential, we created a biophysically realistic model complete with DSM-specific ion channels, such as L- and T-type calcium channels, voltage-gated potassium channels (KDR and KCNQ), IH channel, IK channel, KATP and leak channel (Mahapatra et al. 2018b), SK channel (Gupta and Manchanda 2016), and an extensive calcium dynamics model with pumps, exchanger, buffers and diffusion (Dave and Manchanda 2017). By abolishing the activity of the BK channel, the amplitude and the width of the simulated AP were enhanced. The channel conductance was linearly decremented in steps of 10% and a graded change in the rmp and in the maximum and minimum potentials of the spike was noted. Furthermore, in the absence of BK channels, the hyperpolarisation phase of the AP was completely eliminated, and an after-depolarisation phase surfaced (Fig. 10). It was estimated that the BK channel current contributed to ∼81% of the total outward current (Fig. 10b and Table 7), which is in accord with experimental findings (Petkov 2012, 2014).

BK channels have been specifically targeted to treat various pathophysiologies. They modulate acquisition and maintenance of fear memory (Sun et al. 2015), on grounds of which they have been propounded as potential sites of action for an antipsychotic drug (Lee and Cui 2010). Similarly, they regulate hormone secretion in endocrine cells, such as pancreatic β-cells (Houamed et al. 2010) and anterior pituitary cells (Van Goor et al. 2001), due to which they could foreseeably be employed in devising treatments for hyperinsulinemia (Houamed et al. 2010). Additionally,

studies on BK channels have further demonstrated their effect on controlling spasticity arising from demyelination due to elevated levels of calcium (Baker et al. 2017). It is suggested that bladder dysfunctions can be alleviated by administering drugs that act on BK channels (Nausch et al. 2014; Petkov 2014; Parajuli et al. 2016). Overactive bladder (OAB) is a dysfunctional condition where the patient suffers from frequent urges to void (Fry and Wu 1998; Meng 2009). Typically, anticholinergic and antimuscarinic drugs are prescribed but these, in most cases, are nonoptimal in their efficacy and specificity (Meng 2009; Petkov 2014; Parajuli et al. 2016).

A specific BK channel opener, mallotoxin (or rottlerin) has been patented for the treatment of hypertension and vasoconstriction related disorders (Marx and Zakharov 2004; Maioli et al. 2009). The drug acts by reducing the dependency of BK channels on intracellular calcium, by shifting the channels' activation curve towards relatively hyperpolarised potentials (Zakharov et al. 2005; Guan et al. 2017). Essentially, under the influence of mallotoxin, the normally voltage-and-calcium activated BK channel behaves like a solely voltage-gated potassium channel. The effect of such a drug on the DSM cell was simulated by markedly reducing the calcium dependency of BK channels and shifting the half-activation voltage by $100\,mV$ towards hyperpolarised potentials. Under this condition, the model successfully elicited an AP and a healthy BK current underlying the AP was observed (Fig. 11 and Table 7). This implies that in the presence of mallotoxin and in the absence of elevated intracellular calcium concentration, BK channels can be activated solely by membrane potential, analogous to the operation of voltage-gated potassium channels. Pathological conditions induce changes in the cell physiology (Fry and Wu 1998), of which expression profiles of ion channels could be considered as one such physiological change. The effect of overexpression of this channel under the influence of mallotoxin was also studied. These predictions can be subjected to experimental tests by administering mallotoxin on DSM cells and comparing the AP elicited with the one obtained under control conditions.

A novel BK channel activator NS19504 has been recently introduced in order to relax a spontaneously active bladder (Nausch et al. 2014). It acts by left-shifting the half-activation voltage of the BK channel by 60 mV, which is similar to how mallotoxin exerts its action. The excitability of the DSM cell model was artificially enhanced such that it elicited spontaneous APs in the absence of a stimulus. Under these imposed conditions, NS19504 successfully stabilized the rmp and no spontaneous APs were generated. Our findings thus lend support to the potential applicability of mallotoxin and NS19504 for the treatment of OAB.

Model limitations and avenues for further investigation While simulating BK currents (Fig. 5), biexponential functions were used in order to mimic the time course of the calcium spark and the calcium influx from VDCCs. However, these functions (6)–(11), by themselves do not provide any physical basis for the sub-membrane calcium dynamics. These biexponential functions were so chosen because they best approximated the trend of intracellular calcium variation. Similar BK current fits were achieved using Gaussian functions, skewed Gaussian functions and alpha functions (not shown). Instead of these pre-defined mathematical functions, if the variation of intracellular calcium concentration was derived from first principles, the derived mathematical function would additionally shed light on the physical basis of calcium handling during the activation of the BK channel. Additionally, those functions could be utilised to make heuristic predictions regarding nanodomain interactions (Engbers et al. 2013) between the BK channel and the cytosolic calcium concentration.

Although the effects of the BK channel model on AP parameters (Table 6) yielded results that were within the reported experimental range (Hayase et al. 2009), one particular parameter, the magnitude, deviated from this range. Moreover, the absolute values of the simulation parameters did not agree with those reported in Hayase et al. (2009, Table 1). One possible reason might be the fact that the experimental recordings of AP were taken from individual cells within the guinea-pig detrusor smooth muscle bundle, whereas these simulations pertain to a single isolated DSM cell. This model could be ported into the DSM syncytium model (Appukuttan et al. 2015) to further investigate the spike and its key parameters.

When exploring the effect of mallotoxin, one marked difference between the control AP and the APs elicited under the influence of mallotoxin was the presence of the hyperpolarising phase in the former (Figs. 10 and 11). This indicates that if the calcium concentration in the cell is low, then despite augmented BK channel conductance, the hyperpolarising phase of the AP will be absent, and an after-depolarisation phase can surface. This prediction can be tested by blocking the BK channel's calcium sources and administering the mallotoxin drug to the DSM cell.

5 Conclusions

In conclusion, we developed a biophysically constrained BK channel model activated by a complex interplay of membrane potential, calcium from RyRs and calcium influx from VDCCs, and not possessing the property of inactivation. The model was validated along several lines

and employed to test existing hypotheses. We also used the model to make experimentally testable predictions.

We compared our models with several Hodgkin-Huxley based and Markov model based muscle-specific models (Moczydlowski and Latorre 1983; Rothberg and Magleby 2000; Tong et al. 2011; Korogod et al. 2014; Kochenov et al. 2015; Mahapatra et al. 2018a, b), and found our model's performance to be superior in comparison to the others (Table 8). Additionally, the execution times taken by the 25-state single-channel BK model (Rothberg and Magleby 2000) were compared with our proposed BK channel model and with our integrated NEURON-based action potential model. It was found that the execution time of the 25-state model alone was 4.50 s, whereas that of our proposed BK channel model was $\sim 53\,ms$, and that of the integrated action potential model was $\sim 11\,s$ thereby reinforcing the adaptability of our proposed BK channel model across multiple scales of execution.

The results and observations of our model are applicable at the channel, cellular and clinical level. At the channel level, the model is able to reproduce the $I - \zeta$ curve, and the disparate currents and I-V profiles reported experimentally. It attempts to provide an insight into the cellular environment that could result in these variable profiles. The sub-membrane calcium variation is interesting to study because this parameter plays a crucial role in activating membrane channels, such as the BK channel. Through this model, we are able to predict sub-membrane calcium dynamics during the BK channel's activation, which can foreseeably be tested experimentally. The model employs aspects of sub-membrane calcium dynamics in order to shed light on the variability in the BK channel's behaviour. At the cellular level, the channel model, when integrated with other ion channel, pump and exchanger models, is able to influence the repolarisation and hyperpolarisation phases of the action potential. The BK channel is known to transiently hyperpolarise the resting membrane potential, when activated by spontaneous openings of the RyRs. This aspect of the model behaviour was also successfully tested. At the clinical level, we have used our model to assess the potential applicability of the drug mallotoxin and BK channel activator NS19504, on DSM cells. Our findings support their proposed application in the treatment of OAB.

Although there are fronts along which our model could be further refined, it could be used in its present state to further our understanding of BK channel operation, and elucidate the workings of the channel under physiological and pathophysiological conditions.

Acknowledgements This work was supported by the Department of Biotechnology (DBT), India (Project No. BT/PR12973/MED/122/47/2016). The authors would like to thank Dr. Vijay Kumar Dave (Government Engineering College, Gandhinagar, India) for providing the complete DSM-specific Calcium Dynamics model.

Compliance with Ethical Standards

Conflict of interests The authors declare that they have no conflict of interest.

Ethical Approval The manuscript does not contain any studies with human participants or animals performed by any of the authors.

References

Appukuttan, S., Brain, K.L., Manchanda, R. (2015). A computational model of urinary bladder smooth muscle syncytium. *Journal of Computational Neuroscience*, *38*(1), 167–187.

Baker, D., Pryce, G., Visintin, C., Sisay, S., Bondarenko, A.I., Vanessa Ho, W.S., Jackson, S.J., Williams, T.E., Al-Izki, S., Sevastou, I., Okuyama, M., Graier, W.F., Stevenson, L.A., Tanner, C., Ross, R., Pertwee, R.G., Henstridge, C.M., Irving, A.J., Schulman, J., Powell, K., Baker, M.D., Giovannoni, G., Selwood, D.L. (2017). Big conductance calcium-activated potassium channel openers control spasticity without sedation. *British Journal of Pharmacology*, *174*(16), 2662–2681.

Berridge, M.J. (2008). Smooth muscle cell calcium activation mechanisms. *The Journal of Physiology*, *586*(21), 5047–5061.

Bolton, T.B., & Imaizumi, Y. (1996). Spontaneous transient outward currents in smooth muscle cells. *Cell Calcium*, *20*(2), 141–152.

Brading, A.F. (2006). Spontaneous activity of lower urinary tract smooth muscles: correlation between ion channels and tissue function. *The Journal of Physiology*, *570*(1), 13–22.

Bygrave, F.L., & Benedetti, A. (1996). What is the concentration of calcium ions in the endoplasmic reticulum? *Cell Calcium*, *19*(6), 547–551.

Carnevale, N., & Hines, M. (2006). *The NEURON book*. Cambridge: Cambridge University Press.

Cheng, H., & Lederer, W.J. (2008). Calcium sparks. *Physiological Reviews*, *88*(4), 1491–1545.

Cox, D., Cui, J., Aldrich, R. (1997). Allosteric gating of a large conductance Ca-activated K+ channel. *The Journal of General Physiology*, *110*(3), 257–281.

Cox, D.H. (2014). Modeling a Ca2+ channel/BKCa channel complex at the single-complex level. *Biophysical Journal*, *107*(12), 2797–2814.

Dave, V., & Manchanda, R. (2017). A computational model of the Ca2+ transients and influence of buffering in guinea pig urinary bladder smooth muscle cells. *Journal of Bioinformatics and Computational Biology*, *15*(03), 1750011–1750027.

Donahue, B.S., & Abercrombie, R.F. (1987). Free diffusion coefficient of ionic calcium in cytoplasm. *Cell Calcium*, *8*(6), 437–448.

Engbers, J.D., Zamponi, G.W., Turner, R.W. (2013). Modeling interactions between voltage-gated Ca2+ channels and KCa1. 1 channels. *Channels*, *7*(6), 524–529.

Fry, C.H., & Wu, C. (1998). The cellular basis of bladder instability. *British Journal of Urology*, *81*(1), 1–8.

Fry, C.H., Wu, C., Sui, G.P. (1998). Electrophysiological properties of the bladder. *International Urogynecology Journal*, *9*(5), 291–298.

Fry, C.H., Cooklin, M., Birns, J., Mundy, A.R. (1999). Measurement of intercellular electrical coupling in guinea-pig detrusor smooth muscle. *The Journal of Urology*, *161*(2), 660–664.

Ganitkevich, V.Y., & Isenberg, G. (1991). Depolarization-mediated intracellular calcium transients in isolated smooth muscle cells of guinea-pig urinary bladder. *The Journal of Physiology*, *435*(1), 187–205.

Geng, Y., & Magleby, K.L. (2015). Single-channel kinetics of BK (Slo1) channels. *Frontiers in Physiology*, *5*(532), 1–24.

Ghatta, S., Nimmagadda, D., Xu, X., O'Rourke, S.T. (2006). Large-conductance, calcium-activated potassium channels: structural and functional implications. *Pharmacology and Therapeutics*, *110*(1), 103–116.

Guan, X., Li, Q., Yan, J. (2017). Relationship between auxiliary gamma subunits and mallotoxin on BK channel modulation. *Scientific Reports*, *7*, 42240–42250.

Gupta, S., & Manchanda, R. (2014). A TANH spline interpolation technique for modelling ion channels: application to BK channels in smooth muscle. *International Journal of Simulation–Systems, Science &, Technology*, *15*(6), 97–109.

Gupta, S., & Manchanda, R. (2016). Computational model of SK channel with reference to calcium dynamics in bladder smooth muscles. In *Proceedings of the 12th IASTED international conference biomedical engineering (BioMed 2016)* (pp. 53–59).

Gupta, S., & Manchanda, R. (2018). Effect of gating charges on mediating the dual activation of BK channels in smooth muscle cells: a computational study. In: *Conference proceedings: 40th annual international conference of the IEEE engineering in medicine and biology society* (pp. 5838–5841). IEEE Engineering in Medicine and Biology Society.

Hashitani, H., & Brading, A.F. (2003). Electrical properties of detrusor smooth muscles from the pig and human urinary bladder. *British Journal of Pharmacology*, *140*(1), 146–158.

Hashitani, H., Brading, A.F., Suzuki, H. (2004). Correlation between spontaneous electrical, calcium and mechanical activity in detrusor smooth muscle of the guinea-pig bladder. *British Journal of Pharmacology*, *141*(1), 183–193.

Hayase, M., Hashitani, H., Kohri, K., Suzuki, H. (2009). Role of K+ channels in regulating spontaneous activity in detrusor smooth muscle in situ in the mouse bladder. *The Journal of Urology*, *181*(5), 2355–2365.

Heppner, T., & Bonev, A. (1997). Ca(2+)-activated K+ channels regulate action potential repolarization in urinary bladder smooth muscle. *American Journal of Physiology-Cell Physiology*, *273*(1), C110–C117.

Herrera, G.M., & Nelson, M.T. (2002). Differential regulation of SK and BK channels by Ca2+ signals from Ca2+ channels and ryanodine receptors in guinea-pig urinary bladder myocytes. *The Journal of Physiology*, *541*(2), 483–492.

Herrera, G.M., Heppner, T.J., Nelson, M.T. (2001). Voltage dependence of the coupling of Ca(2+) sparks to BK(Ca) channels in urinary bladder smooth muscle. *American Journal of Physiology Cell Physiology*, *280*(3), C481–90.

Hirano, M., Imaizumi, Y., Muraki, K., Yamada, A., Watanabe, M. (1998). Effects of ruthenium red on membrane ionic currents in urinary bladder smooth muscle cells of the guinea-pig. *Pflugers Archiv*, *435*(5), 645–653.

Hollywood, M.A., McCloskey, K.D., McHale, N.G., Thornbury, K.D. (2000). Characterization of outward K(+) currents in isolated smooth muscle cells from sheep urethra. *American Journal of Physiology-Cell Physiology*, *279*(2), C420–C428.

Houamed, K.M., Sweet, I.R., Satin, L.S. (2010). BK Channels mediate a novel ionic mechanism that regulates glucose-dependent electrical activity and insulin secretion in mouse pancreatic β-cells. *The Journal of Physiology*, *588*(18), 3511–3523.

Hristov, K.L., Chen, M., Kellett, W.F., Rovner, E.S., Petkov, G.V. (2011). Large-conductance voltage- and Ca2+-activated K+ channels regulate human detrusor smooth muscle function. *American Journal of Physiology-Cell Physiology*, *301*(4), C903–C912.

Jaffe, D.B., Wang, B., Brenner, R. (2011). Shaping of action potentials by type I and type II large-conductance Ca2+-activated K+ channels. *Neuroscience*, *192*, 205–218.

Jaggar, J.H., Porter, V.A., Lederer, W.J., Nelson, M.T. (2000). Calcium sparks in smooth muscle. *American Journal of Physiology-Cell Physiology*, *278*(2), C235–C256.

Kaczorowski, G.J., & Garcia, M.L. (1999). Pharmacology of voltage-gated and calcium-activated potassium channels. *Current Opinion in Chemical Biology*, *3*(4), 448–458.

Klöckner, U., & Isenberg, G. (1985). Action potentials and net membrane currents of isolated smooth muscle cells (urinary bladder of the guinea-pig). *Pflügers Archiv European Journal of Physiology*, *405*(4), 329–339.

Kobayter, S., Young, J.S., Brain, K.L. (2012). Prostaglandin E2 induces spontaneous rhythmic activity in mouse urinary bladder independently of efferent nerves. *British Journal of Pharmacology*, *165*(2), 401–413.

Kochenov, A.V., Poddubnaya, E.P., Makedonsky, I.A., Korogod, S.M. (2015). Biophysical processes in a urinary bladder detrusor smooth muscle cell during rehabilitation electrostimulation: a simulation study. *Neurophysiology*, *47*(3), 174–184.

Korogod, S., Kochenov, A., Makedonsky, I. (2014). Biophysical mechanism of parasympathetic excitation of urinary bladder smooth muscle cells: a simulation study. *Neurophysiology*, *46*(4), 293–299.

Kyle, B.D., Bradley, E., Large, R., Sergeant, G.P., McHale, N.G., Thornbury, K.D., Hollywood, M.A. (2013). Mechanisms underlying activation of transient BK current in rabbit urethral smooth muscle cells and its modulation by IP3-generating agonists. *American Journal of Physiology-Cell Physiology*, *305*(6), C609–C622.

Laver, D.R., & Lamb, G.D. (1998). Inactivation of Ca2+ release channels (ryanodine receptors RyR1 and RyR2) with rapid steps in [Ca2+] and voltage. *Biophysical Journal*, *74*(5), 2352–2364.

Lee, U.S., & Cui, J. (2010). BK channel activation: Structural and functional insights. *Trends in Neurosciences*, *33*(9), 415–423.

Lifshitz, L.M., Carmichael, J.D., Lai, F.A., Sorrentino, V., Bellvé, K., Fogarty, K.E., ZhuGe, R. (2011). Spatial organization of RYRs and BK channels underlying the activation of STOCs by Ca2+ sparks in airway myocytes. *The Journal of General Physiology*, *138*(2), 195–209.

Lovell, P.V., James, D.G., McCobb, D.P. (2000). Bovine versus rat adrenal chromaffin cells: big differences in BK potassium channel properties. *Journal of Neurophysiology*, *83*(6), 3277–3286.

Luo, C.-H., & Rudy, Y. (1994). A dynamic model of the cardiac ventricular action potential. I. Simulations of ionic currents and concentration changes. *Circulation Research*, *74*(6), 1071–1096.

Magleby, K.L. (2003). Gating mechanism of BK (Slo1) channels: so near, yet so far. *The Journal of General Physiology*, *121*(2), 81–96.

Mahapatra, C., Brain, K., Manchanda, R. (2018a). Computational study of Hodgkin-Huxley type calcium-dependent potassium current in urinary bladder over activity. In: *2018 IEEE 8th international conference on computational advances in bio and medical sciences (ICCABS)* (pp. 1–4). IEEE.

Mahapatra, C., Brain, K.L., Manchanda, R. (2018b). A biophysically constrained computational model of the action potential of mouse urinary bladder smooth muscle. *PloS One*, *13*(7), e0200712.

Maioli, E., Greci, L., Soucek, K., Hyzdalova, M., Pecorelli, A., Fortino, V., Valacchi, G. (2009). Rottlerin inhibits ROS formation and prevents NFκB activation in MCF-7 and HT-29 cells. *Journal of Biomedicine and Biotechnology*, *2009*, 1–7.

Mandge, D., & Manchanda, R. (2018). A biophysically detailed computational model of bladder small DRG neuron soma. *PLoS Computational Biology*, *14*(7), e1006293.

Marx, S.O., & Zakharov, S.I. (2004). Use of rottlerin and its derivatives as activators of BK channel for therapy of hypertension and related disorders. https://patents.google.com/patent/WO2006060196A2/en.

MATLAB (2018). R2018a. The MathWorks Inc., Natick, Massachusetts.

McDougal, R.A., Morse, T.M., Carnevale, T., Marenco, L., Wang, R., Migliore, M., Miller, P.L., Shepherd, G.M., Hines, M.L. (2017). Twenty years of ModelDB and beyond: building essential modeling tools for the future of neuroscience. *Journal of Computational Neuroscience*, *42*(1), 1–10.

Meech, R.W., & Standen, N.B. (1975). Potassium activation in *Helix Aspersa* neurones under voltage clamp: a component mediated by calcium influx. *The Journal of Physiology*, *249*(2), 211–259.

Meng, E. (2009). Recent research advances in the pathophysiology of overactive bladder. *Incont Pelvic Floor Dysfunct*, *3*(Suppl 1), 5–7.

Meredith, A.L., Thorneloe, K.S., Werner, M.E., Nelson, M.T., Aldrich, R.W. (2004). Overactive bladder and incontinence in the absence of the BK large conductance Ca2+-activated K+ channel. *Journal of Biological Chemistry*, *279*(35), 36746–36752.

Mijailovich, S.M., Nedic, D., Svicevic, M., Stojanovic, B., Walklate, J., Ujfalusi, Z., Geeves, M.A. (2017). Modeling the actin myosin ATPase cross-bridge cycle for skeletal and cardiac muscle myosin isoforms. *Biophysical Journal*, *112*(5), 984–996.

Moczydlowski, E., & Latorre, R. (1983). Gating kinetics of Ca2+-activated K+ channels from rat muscle incorporated into planar lipid bilayers. Evidence for two voltage-dependent Ca2+ binding reactions. *The Journal of General Physiology*, *82*(4), 511–542.

Nausch, B., Rode, F., Jorgensen, S., Nardi, A., Korsgaard, M.P.G., Hougaard, C., Bonev, A.D., Brown, W.D., Dyhring, T., Strobaek, D., Olesen, S.-P., Christophersen, P., Grunnet, M., Nelson, M.T., Ronn, L.C.B. (2014). NS19504: A novel BK channel activator with relaxing effect on bladder smooth muscle spontaneous phasic contractions. *Journal of Pharmacology and Experimental Therapeutics*, *350*(3), 520–530.

Orio, P., Yolima, T., Patricio, R., Carvacho, I., Garcia, M.L., Toro, L., Valverde, M.A., Latorre, R. (2006). Structural determinants for functional coupling between the β and α subunits in the Ca2+-activated K+ (BK) channel. *The Journal of General Physiology*, *127*(2), 191–204.

Parajuli, S.P., Hristov, K.L., Cheng, Q., Malysz, J., Rovner, E.S., Petkov, G.V. (2015). Functional link between muscarinic receptors and large-conductance Ca2+-activated K+ channels in freshly-isolated human detrusor smooth muscle cells. *Pflügers Archiv-European Journal of Physiology*, *467*(4), 665–675.

Parajuli, S.P., Zheng, Y.-M., Levin, R., Wang, Y.-X. (2016). Big-conductance Ca2+-activated K+ channels in physiological and pathophysiological urinary bladder smooth muscle cells. *Channels*, *10*(5), 355–364.

Petkov, G.V. (2012). Role of potassium ion channels in detrusor smooth muscle function and dysfunction. *Nature Reviews Urology*, *9*(1), 30–40.

Petkov, G.V. (2014). Central role of the BK channel in urinary bladder smooth muscle physiology and pathophysiology. *American Journal of Physiology - Regulatory Integrative and Comparative Physiology*, *307*(6), R571–R584.

Petkov, G.V., & Nelson, M.T. (2005). Differential regulation of Ca2+-activated K+ channels by β-adrenoceptors in guinea pig urinary bladder smooth muscle. *American Journal of Physiology-Cell Physiology*, *288*(6), C1255–C1263.

Prosser, C.L. (1974). Smooth muscle. *Annual Review of Physiology*, *36*(1), 503–535.

Rothberg, B.S., & Magleby, K.L. (2000). Voltage and Ca2+ activation of single large-conductance Ca2+-activated K+ channels described by a two-tiered allosteric gating mechanism. *The Journal of General Physiology*, *116*(1), 75–100.

Salkoff, L., Butler, A., Ferreira, G., Santi, C., Wei, A. (2006). High-conductance potassium channels of the SLO family. *Nature Reviews Neuroscience*, *7*(12), 921–931.

Spiess, A.-N., & Neumeyer, N. (2010). An evaluation of R^2 as an inadequate measure for nonlinear models in pharmacological and biochemical research: A Monte Carlo approach. *BMC Pharmacology*, *10*(6), 1–11.

Steephen, J.E., & Manchanda, R. (2009). Differences in biophysical properties of nucleus accumbens medium spiny neurons emerging from inactivation of inward rectifying potassium currents. *Journal of Computational Neuroscience*, *27*(3), 453–470.

Sui, G.P., Wu, C., Fry, C.H. (2001). The electrophysiological properties of cultured and freshly isolated detrusor smooth muscle cells. *The Journal of Urology*, *165*(2), 627–632.

Sun, P., Zhang, Q., Zhang, Y., Wang, F., Wang, L., Yamamoto, R., Sugai, T., Kato, N. (2015). Fear conditioning suppresses large-conductance calcium-activated potassium channels in lateral amygdala neurons. *Physiology and Behavior*, *138*, 279–284.

Tong, W.C., Choi, C.Y., Kharche, S., Holden, A.V., Zhang, H., Taggart, M.J. (2011). A computational model of the ionic currents, Ca2+ dynamics and action potentials underlying contraction of isolated uterine smooth muscle. *PloS One*, *6*(4), e18685.

Turner, W.H., & Brading, A.F. (1997). Smooth muscle of the bladder in the normal and the diseased state: pathophysiology, diagnosis and treatment. *Pharmacology and Therapeutics*, *75*(2), 77–110.

Van Goor, F., Zivadinovic, D., Stojilkovic, S.S. (2001). Differential expression of ionic channels in rat anterior pituitary cells. *Molecular Endocrinology*, *15*(7), 1222–1236.

Vergara, C., Latorre, R., Marrion, N.V., Adelman, J.P. (1998). Calcium-activated potassium channels. *Current Opinion in Neurobiology*, *8*(3), 321–329.

Zakharov, S.I., Morrow, J.P., Liu, G., Yang, L., Marx, S.O. (2005). Activation of the BK (SLO1) potassium channel by mallotoxin. *Journal of Biological Chemistry*, *280*(35), 30882–30887.